

1 Controls on the stable isotope compositions of travertine from hyperalkaline springs in
2 Oman: Insights from clumped isotope measurements
3
4 E.S. Falk ^{a*}, W. Guo ^a, A.N. Paukert ^{b,c}, J.M. Matter ^{b,d}, E.M. Mervine ^{a,e}, P.B. Kelemen ^b

^a Woods Hole Oceanographic Institution, 266 Woods Hole Road, Woods Hole, MA 02543, USA

^b Lamont-Doherty Earth Observatory, Columbia University, 61 Route 9W, Palisades, NY 10964, USA

^c California State University Sacramento, 6000 J Street, Sacramento, CA 95819, USA.

^d University of Southampton, University Road, Southampton SO17 1BJ, UK

^e De Beers Marine, Golf Park 2, Raapenberg Road, Pinelands, 7405, Cape Town, South Africa

*Corresponding author. Current address: North Carolina State University, 2800 Faucette Drive, Raleigh, NC 27695, USA. esfalk@ncsu.edu. +1 919 515 3711

5 **Abstract**

6 Carbonate formation at hyperalkaline springs is typical of serpentinization in
7 peridotite massifs worldwide. These travertines have long been known to exhibit large
8 variations in their carbon and oxygen isotope compositions, extending from apparent
9 equilibrium values to highly depleted values. However, the exact causes of these
10 variations are not well constrained. We analyzed a suite of well-characterized fresh
11 carbonate precipitates and travertines associated with hyperalkaline springs in the
12 peridotite section of the Samail ophiolite, Sultanate of Oman, and found their clumped
13 isotope compositions vary systematically with formation environments. Based on these
14 findings, we identified four main processes controlling the stable isotope compositions of
15 these carbonates. These include hydroxylation of CO₂, partial isotope equilibration of
16 dissolved inorganic carbon, mixing between isotopically distinct carbonate end-members,
17 and post-depositional recrystallization. Most notably, in fresh crystalline films on the
18 surface of hyperalkaline springs and in some fresh carbonate precipitates from the bottom
19 of hyperalkaline pools, we observed large enrichments in Δ_{47} (up to ~0.2‰ above
20 expected equilibrium values) which accompany depletions in $\delta^{18}\text{O}$ and $\delta^{13}\text{C}$, yielding
21 about 0.01‰ increase in Δ_{47} and 1.1‰ decrease in $\delta^{13}\text{C}$ for every 1‰ decrease in $\delta^{18}\text{O}$,
22 relative to expected equilibrium values. This disequilibrium trend, also reflected in
23 preserved travertines ranging in age from modern to ~40,000 years old, is interpreted to
24 arise mainly from the isotope effects associated with the hydroxylation of CO₂ in high-
25 pH fluids and agrees quantitatively with our theoretical prediction. In addition, in some
26 fresh carbonate precipitates from the bottom of hyperalkaline pools and in subsamples of
27 one preserved travertine terrace, we observed additional enrichments in Δ_{47} at

28 intermediate $\delta^{13}\text{C}$ and $\delta^{18}\text{O}$, consistent with mixing between isotopically distinct
29 carbonate end-members. Our results suggest that carbonate clumped isotope analysis can
30 be a valuable tool for identifying and distinguishing processes not readily apparent from
31 the carbonate bulk stable isotope compositions alone, e.g., kinetic effects or mixing of
32 different carbonate end-members, which can significantly alter both the apparent
33 formation temperatures and apparent radiocarbon ages. The isotope trends observed in
34 these travertine samples could be applied more broadly to identify extinct hyperalkaline
35 springs in terrestrial and extraterrestrial environments, to better constrain the formation
36 conditions and post-depositional alteration of hyperalkaline spring carbonates, and to
37 extract potential paleoclimate information.

38

39 **1. Introduction**

40 **1.1 Carbonate formation in peridotite-hosted hyperalkaline springs**

41 Springs emanating from serpentinized peridotite in the Samail ophiolite, Sultanate
42 of Oman, are characterized by high pH (~11-12), high Ca^{2+} concentrations, and almost no
43 dissolved inorganic carbon (DIC). These hyperalkaline springs react with atmospheric
44 CO_2 , resulting in rapid precipitation of calcium carbonate and formation of extensive
45 travertine terraces (Neal and Stanger 1985; Clark and Fontes, 1990; Kelemen and Matter,
46 2008; Matter and Kelemen, 2009; Kelemen et al., 2011; Paukert et al., 2012; Chavagnac
47 et al. 2013a,b; Mervine et al., 2014, 2015).

48 The development of these Ca^{2+} - OH^- rich waters is typical of serpentinization in
49 peridotite massifs worldwide (e.g., Barnes et al., 1967; Barnes and O'Neil, 1969; Barnes
50 et al., 1978; Neal and Stanger, 1985; Bruni et al., 2002; Neal and Shand, 2002; Marques

51 et al., 2008; Szponar et al., 2013; Cardace et al., 2015). Such ultramafic systems have
52 been the subject of diverse studies, with much interest in fate of carbon in these
53 environments. The rapid uptake of CO₂ during natural carbonation of peridotite,
54 estimated to currently be $\sim 10^3$ tons of CO₂ km⁻³ yr⁻¹ in Oman, has been viewed as a
55 promising analog for mineral carbon sequestration (e.g., Cipolli et al., 2004; Kelemen
56 and Matter, 2008; Wilson et al., 2009). The development of hyperalkaline fluids during
57 serpentinization has also been suggested as possible driver of carbonate precipitation and
58 methane generation on Mars (e.g., Niles et al., 2005; Oze and Sharma, 2005; Ehlmann et
59 al., 2010; Etiope et al., 2013), attracting attention to terrestrial hyperalkaline springs as
60 potential Martian analogs (e.g., Szponar et al., 2013). In addition, there have been
61 attempts to reconstruct paleoclimate in Oman (e.g. periods of aridity or humidity) based
62 on variations in travertine morphology and the bulk stable isotope compositions of
63 carbonates (Clark and Fontes, 1990).

64 Unlike typical travertines precipitated by degassing of CO₂ from calcium- and
65 bicarbonate-rich waters of hydrothermal origin, which may record apparent equilibrium
66 oxygen and clumped isotope compositions near spring vents (e.g., Kele et al., 2015), the
67 isotope compositions of travertines formed at hyperalkaline springs usually deviate
68 significantly from expected equilibrium values. Previous studies of peridotite-hosted
69 travertines in Oman revealed positive correlations between their $\delta^{13}\text{C}$ and $\delta^{18}\text{O}$ values,
70 with $\delta^{13}\text{C}$ vs. $\delta^{18}\text{O}$ slope of ~ 1.3 (Clark and Fontes, 1990; Clark et al., 1992; Kelemen et
71 al., 2011; Mervine et al., 2014). The youngest travertines are often characterized by large
72 depletions in ¹³C and ¹⁸O (Clark et al., 1992; Kelemen et al., 2011; Mervine et al., 2014),
73 while preserved travertines generally exhibit relatively higher $\delta^{13}\text{C}$ and $\delta^{18}\text{O}$ values that

74 may extend to values consistent with expected equilibrium with observed spring-water
75 $\delta^{18}\text{O}$ and temperatures and atmospheric $\delta^{13}\text{C}$ (Neal and Stanger, 1985; Clark et al., 1992;
76 Matter, 2005). Similar correlated depletions in $\delta^{13}\text{C}$ and $\delta^{18}\text{O}$ have been observed
77 worldwide in other carbonates precipitated during interaction between alkaline waters
78 and atmospheric CO_2 . For example, the $\delta^{13}\text{C}$ and $\delta^{18}\text{O}$ values of fresh carbonate
79 precipitates and travertines from hyperalkaline springs in northern California overlap
80 significantly with values observed in Oman (O'Neil and Barnes, 1971; Kelemen et al.,
81 2011). These depletions in $\delta^{13}\text{C}$ and $\delta^{18}\text{O}$ have typically been interpreted as a kinetic
82 isotope effect resulting from CO_2 uptake from the atmosphere (O'Neil and Barnes, 1971;
83 Clark et al., 1992; Wilson et al., 2010). In some cases depleted isotopic signatures in
84 carbonates precipitated in alkaline environments may also be derived from nearby
85 carbonate sediments, as was initially suggested for surface calcium carbonates associated
86 with weathering of chrysotile tailings in northern British Columbia (Wilson et al., 2009).
87

88 **1.2 Carbonate clumped isotope geochemistry**

89 The carbonate clumped isotope thermometer is a relatively new paleothermometer
90 based on the tendency of ^{13}C and ^{18}O isotopes to preferentially bond to one another (or
91 “clump”) within the CO_3^{2-} groups under thermodynamic equilibrium. This property is
92 commonly measured as ‘ Δ_{47} ,’ the excess of mass-47 isotopologue (primarily $^{13}\text{C}^{18}\text{O}^{16}\text{O}$)
93 in the CO_2 evolved from phosphoric acid digestion of solid carbonate relative to the
94 abundances expected for a stochastic distribution of all isotopes (Ghosh et al., 2006;
95 Eiler, 2007; Eiler, 2011; Huntington et al., 2009):

96

97 $\Delta_{47} = \left[\left(\frac{R_{47}}{R_{47}^*} - 1 \right) - \left(\frac{R_{46}}{R_{46}^*} - 1 \right) - \left(\frac{R_{45}}{R_{45}^*} - 1 \right) \right] \times 1000$ (Equation 1a)

98 where R_i is the measured ratio of the isotopologue of mass i and R_i^* is the ratio for a

99 stochastic distribution. i.e., $\Delta_{47} = \left[\frac{R_{47}}{2R_{13} \times R_{18} + 2R_{17} \times R_{18} + R_{13} \times (R_{17})^2} - \right.$

100 $\left. \frac{R_{46}}{2R_{18} + 2R_{13} \times R_{17} + (R_{17})^2} - \frac{R_{45}}{R_{13} + 2R_{17}} + 1 \right] \times 1000$ (Equation 1b).

101

102 Unlike conventional carbonate-water oxygen isotope thermometry, the extent of this
 103 clumping effect, under thermodynamic equilibrium, depends only on the equilibration
 104 temperature and not on the isotopic composition of the waters from which the carbonate
 105 precipitated. This makes it a valuable tool for a variety of applications, especially in cases
 106 where the isotopic composition of the parent waters are difficult to constrain, e.g.
 107 paleoclimate, paleoaltimetry, diagenesis, and low grade metamorphism (see reviews in
 108 Eiler, 2011; Affek, 2012; Huntington and Lechler, 2015).

109 Although inter-laboratory differences remain in the calibration of the carbonate
 110 clumped isotope paleothermometer, calibrations among a variety of natural and synthetic
 111 carbonates have so far yielded remarkably consistent results within individual
 112 laboratories considering the range of materials studied (e.g., Ghosh et al., 2006; Dennis
 113 and Schrag, 2010; Tripathi et al., 2010; Eiler, 2011; Eagle et al., 2013; Grauel et al., 2013;
 114 Henkes et al., 2013; Zaarur et al., 2013; Defliese et al., 2015; Kele et al., 2015; Kluge et
 115 al., 2015). Mostly notably, the clumped isotope compositions of some carbonate
 116 materials that were known to be affected by kinetic effects in bulk stable isotopes, such as
 117 certain deep-sea corals, foraminifera and coccoliths, appear to conform to the equilibrium
 118 temperature calibration relationship derived from inorganic carbonates precipitated in the

119 laboratory (e.g., Tripathi et al., 2010; Thiagarajan et al., 2011). However, there is
120 increasing evidence that disequilibrium clumped isotope effects also exist in nature,
121 especially for several types of carbonates, e.g. speleothems, cryogenic carbonates (e.g.,
122 Affek et al., 2008; Guo 2008; Daeron et al., 2011; Wainer et al., 2011; Kluge and Affek,
123 2012; Kluge et al., 2014; Affek et al., 2014), some shallow-water and cold-water corals
124 (Saenger et al., 2012; Spooner et al., 2016). These disequilibrium clumped isotope
125 effects, if not corrected for, would lead to systematic over-estimation (e.g. for
126 speleothems and cryogenic carbonates) or under-estimation (e.g. for some corals) of the
127 carbonate formation temperatures derived from the clumped isotope thermometer. Our
128 current understanding of the causes of these disequilibrium effects is still limited, but
129 most of these effects are thought to be related to the kinetic isotope fractionations
130 associated with the CO₂ hydration/hydroxylation reactions and their reverse reactions
131 (e.g., Guo, 2008; Saenger et al., 2012; Affek et al., 2014; Spooner et al., 2016). The same
132 reactions, particularly CO₂ hydroxylation, play key roles in carbonate formation during
133 rapid uptake of CO₂ at alkaline springs, as in Oman (Clark et al., 1992). Here we present
134 an investigation of the clumped isotope systematics of carbonates formed in
135 hyperalkaline springs in Oman, and discuss the implication of our findings for the
136 interpretation of the isotopic compositions of travertines formed in similar environments.
137

138 **2. Geologic setting and travertine formation in Oman**

139 The Samail ophiolite, in the Sultanate of Oman and the United Arab Emirates
140 (Figure 1), represents one of the largest exposures of mantle peridotite on land. The
141 mantle peridotite section is composed of residual harzburgites and dunites and is variably

142 serpentized, typically ~30-80% (e.g., Boudier and Coleman, 1981; Godard et al., 2000;
143 Monnier et al., 2006; Hanghøj et al., 2010), with completely serpentized peridotite
144 commonly observed in more altered sections. Much of this serpentine is thought to have
145 formed during suboceanic hydrothermal alteration prior to exposure of the ophiolite on
146 land (e.g., Boudier et al., 2010), but low temperature serpentization continues today
147 during reaction of meteoric water with peridotite (e.g., Barnes and O'Neil, 1978; Neal
148 and Stanger, 1983; Streit et al., 2012).

149 This ongoing low temperature alteration of peridotite leads to the formation of
150 hyperalkaline springs and abundant carbonate precipitation via three steps. (1) Meteoric
151 surface waters react with shallow peridotite in an open system that remains in equilibrium
152 with atmospheric CO₂ and O₂. This results in the formation of waters rich in Mg²⁺-
153 HCO₃⁻, also known as “Type I” waters (Barnes and O'Neil, 1969). (2) As surface waters
154 percolate deeper into the peridotite, they become isolated from the atmosphere. The
155 formation of Mg-rich alteration products, such as serpentine and Mg-carbonate, in this
156 subsurface environment leads to decreases in concentrations of Mg²⁺ and DIC, while Ca²⁺
157 continues to accumulate in the groundwater through continued dissolution of peridotite.
158 This results in the formation of alkaline Ca²⁺-OH⁻ waters, also known as “Type II”
159 waters, characterized by high pH (up to 12), low Eh (approximately -200 mV), and
160 virtually no Mg²⁺ (typically <10⁻² mmol/L) or DIC (typically ~10⁻¹ mmol/L) (Barnes and
161 O'Neil, 1969; Neal and Stanger, 1985; Bruni et al., 2002; Paukert et al., 2012; Chavagnac
162 et al., 2013b). (3) When these Ca²⁺-OH⁻ waters reach the surface as hyperalkaline
163 springs, rapid precipitation of calcium carbonate results from reaction with CO₂, either by

164 direct uptake of atmospheric CO₂ or mixing with shallow groundwater or surface waters
165 containing ~3-5 mmol/L DIC (Paukert et al., 2012).

166 Alkaline springs of this type are common throughout the peridotite section of the
167 Samail ophiolite, with close to 100 such springs identified in previous studies (e.g.,
168 Stanger, 1985; Neal and Stanger, 1985; Kelemen and Matter, 2008; Paukert et al., 2012;
169 Chavagnac et al., 2013b). Where alkaline spring water comes in contact with atmospheric
170 CO₂, crystalline films of calcium carbonate may form on the surface of pools. This
171 reaction is rapid enough that calcium carbonate crusts ~0.5mm thick re-form on the
172 surface of the pools within a couple days when they are removed by rainstorms or
173 manually. In many locations, these alkaline springs form a series of striking, milky-blue
174 pools lined with white unconsolidated calcium carbonate precipitates, particularly where
175 springs emerge along wadi (stream) beds. Alkaline spring water may also flow along the
176 surface of travertine terraces in shallow trickles without the development of larger pools
177 or may form speleothem-like carbonate structures where eroded peridotite outcrops form
178 overhangs that allow alkaline water to drip freely. In previous studies of carbonate
179 mineralogy at alkaline springs, fresh calcium carbonate precipitates have been found to
180 be mixtures of calcite and aragonite, with calcite more common in surface films and
181 aragonite more common in bottom deposits (Paukert et al., 2012; Chavagnac et al.,
182 2013a; Mervine et al., 2014).

183 Over time, calcium carbonate precipitation associated with these hyperalkaline
184 springs has resulted in the build-up of extensive travertine terraces, typically ~200,000 m²
185 in area and ~1 m thick, in areas surrounding active springs (Kelemen and Matter, 2008).
186 Radiometric dating and measurements of layer thickness within travertine terraces

187 suggests that travertine deposition has been ongoing for at least 50,000 years, with
188 average deposition rates of ~0.1-0.3 mm/year (Kelemen and Matter, 2008; Mervine et al.,
189 2014). Clark and Fontes (1990) had previously argued that surficial travertine deposits in
190 Oman were only deposited and preserved during periods of hyper-aridity, but subsequent
191 studies have identified travertine terraces with ^{14}C ages that fill in the gaps in the Clark
192 and Fontes (1990) record (Kelemen and Matter, 2008; Mervine et al., 2014).

193

194 **3. Material and Methods**

195 **3.1 Description of carbonate samples**

196 A total of 29 samples of fresh carbonate precipitates from alkaline springs and 14
197 preserved travertines were collected from 9 locations throughout the southern portion of
198 the Samail ophiolite (Figure 1) over several field seasons, each January between 2007
199 and 2012. Sample locations and descriptions are presented in Table 1, and photos of some
200 sampling locations are shown in Figure 2. Many of these samples (10 fresh carbonate
201 precipitates and 14 travertines, as indicated in Table 1) have been included in previous
202 studies of hyperalkaline springs and travertine formation in Oman, in which their
203 mineralogical composition, carbon and oxygen isotope composition, and/or ^{14}C ages were
204 reported (Kelemen et al., 2011; Paukert et al., 2012; Falk, 2013; Mervine et al., 2014).
205 None of the samples have been analyzed before for their clumped isotope compositions.
206 In this study, we performed clumped isotope analysis on 28 of these carbonate samples
207 and only bulk carbon and oxygen isotope analysis on the other 15 samples.

208 The fresh carbonate precipitates we collected from hyperalkaline springs can be
209 grouped into two main types: (1) “surface films”—thin crystalline films or crusts formed

210 at the surface of hyperalkaline springs (e.g., Figure 2c)—and (2) “bottom floc”—the
211 unconsolidated carbonate lining hyperalkaline spring pools and outlet channels. Bottom
212 floc samples can be further divided based on their depositional environments. Some are
213 found in larger hyperalkaline spring pools within wadi (stream) beds (e.g., Figure 2a),
214 while others form in smaller pools and thin flows along the surface of travertine terraces
215 (e.g., Figure 2b,d). All surface films were collected directly at the hyperalkaline spring
216 source. Bottom floc samples were collected either directly at the hyperalkaline spring
217 source or at downstream locations close enough to the spring that water pH remained
218 above 11. Carbonates collected at the exact same location as water samples are listed
219 with their corresponding water samples in Table 2. These include “flow path” samples—
220 samples collected downstream from the alkaline spring outlet, with distance from the
221 spring indicated in Table 2.

222 The travertine samples in this study include recently-formed travertine layers
223 from areas of active travertine deposition and older laminated travertine terraces (Figure
224 2f). Specifically, the older travertine samples consist of carefully subsampled layers of a
225 ~2m thick travertine section from Al Bana (i.e., the Misht Travertine location; Mervine et
226 al. 2014) and a ~1m thick travertine section from the Wadi Uqaybah travertine, both of
227 which were previously described and radiocarbon dated by Mervine et al. (2014). There
228 are no active hyperalkaline springs flowing along the surfaces of these older travertines
229 where these samples were collected, but they are located in the general vicinity of active
230 hyperalkaline springs.

231 Sample collection and processing methods for fresh precipitates, preserved
232 travertines, and associated water samples are described in detail by Paukert et al. (2012)

233 and Mervine et al. (2014). Briefly, fresh precipitates collected from hyperalkaline pools
234 were allowed to dry at ambient conditions and later dried in a 40°C oven. Because of the
235 very fine-grained nature of these precipitates, crushing and mechanical powdering of
236 these samples was not necessary prior to mineralogical and isotopic analyses. Preserved
237 travertine rock samples collected in 2007-2009 were crushed in a jaw crusher and
238 powdered in a puck mill or with an agate mortar and pestle. Layers from travertines
239 collected in 2010 were carefully subsampled at millimeter scales using a micromill, as
240 previously described in Mervine et al. (2014).

241

242 **3.2 Properties of spring water**

243 In situ and laboratory-based measurements were made on spring water from
244 hyperalkaline pools and flow paths along the surface of travertine terraces, to determine
245 water temperature, pH, major element chemistry and stable isotopic compositions (Table
246 2). These field data and water samples were obtained in 2008-2012 (year of collection
247 indicated by sample prefix), during the same field seasons as the carbonate samples
248 described above, and several pools (“sites”) were re-visited over the course of multiple
249 field seasons. Many of the fresh carbonate samples discussed in this study were collected
250 from the same pools as the spring water samples, as indicated in Table 2. In most of those
251 cases, collection of water samples and in situ measurements of pH were made at the time
252 of collection of fresh carbonate precipitates. Additional data for some of the water
253 samples (e.g., conductivity, oxidation-reduction potential, and major and trace element
254 concentrations) have been reported previously in Paukert et al. (2012), as indicated in
255 Table 2.

256 In situ measurements of the pH and temperature of alkaline springs were
257 conducted using a WTW Multi 3400i multi-parameter field meter (Paukert et al., 2012).
258 Major cation compositions were determined by inductively coupled plasma atomic
259 emission spectrometry (ICP-AES) on a Horiba Jobin-Yvon Activa M spectrometer at
260 Columbia University, by inductively coupled plasma atomic absorption spectrometry on
261 a Perkin-Elmer AAnalyst 800 spectrometer at CUNY Queens College, and an inductively
262 coupled plasma mass spectrometer at Arizona State University. DIC concentrations were
263 measured at Arizona State University on an OI Analytical Model 1010 Wet Oxidation
264 TOC Analyzer for samples from the 2009 and 2010 field season and at Columbia
265 University via acidification on a UIC CM5230 carbon analyzer for samples from the
266 2012 field season. The analytical precisions were $\pm 2\%$ and $\pm 1\%$ (relative standard
267 deviation) for major cation concentrations and DIC concentration measurements,
268 respectively.

269 $\delta^{18}\text{O}$ and δD of water, and $\delta^{13}\text{C}$ of DIC were measured by isotope ratio mass
270 spectrometry (IRMS) in the Environmental Isotopes Laboratory at the University of
271 Waterloo. $\delta^{18}\text{O}$ of water was determined by the CO_2 equilibration method (Epstein and
272 Mayeda, 1953), using a VG 903 mass spectrometer for samples from the 2008 field
273 season (prefix "OM08-") and using a Micromass IsoPrime mass spectrometer for all
274 other samples. δD of water was analyzed by the chromium reduction method on a
275 Eurovector Euro 3000 Elemental Analyzer coupled to a Micromass IsoPrime mass
276 spectrometer (Gehre et al., 1996). For carbon isotope measurements of DIC, water was
277 reacted under vacuum with anhydrous (100%) H_3PO_4 (McCrea, 1950), and the liberated
278 CO_2 was then directly released into a Micromass IsoPrime mass spectrometer via a

279 Gilson 222XL auto-sampler. The overall analytical precisions were $\pm 0.2\%$, $\pm 0.8\%$, and
280 $\pm 0.2\%$ (1 S. D.) for $\delta^{18}\text{O}_{\text{water}}$, δD , and $\delta^{13}\text{C}_{\text{DIC}}$, respectively. The isotopic data are
281 reported relative to Vienna Standard Mean Ocean Water (VSMOW) and Vienna Pee-Dee
282 Belemnite (VPDB).

283

284 **3.3 Carbonate mineral identification**

285 For fresh carbonate precipitates collected in 2012 that were subject to clumped
286 isotope analysis, calcium carbonate minerals were identified by Raman spectroscopy
287 using a Horiba LabRAM HR confocal Raman spectrometer at Woods Hole
288 Oceanographic Institution (WHOI). Spectra were collected for 5 s with 3 accumulations
289 averaged for each analysis spot. Each sample was analyzed at four spots and each
290 spectrum was classified as calcite, aragonite, or a very fine-grained mixture of both in
291 order to reflect the relative proportions of each mineral.

292 The mineralogy of samples collected in 2007-2011 was determined by powder X-
293 ray diffraction (XRD) and reported in detail in previous studies (Kelemen et al., 2011;
294 Paukert et al., 2012; Falk, 2013; and Mervine et al., 2014). Semi-quantitative estimates of
295 mineral proportions based on relative peak intensities of X-ray diffraction spectra were
296 used to classify each mineral as major ($> \sim 20\%$) or minor ($< \sim 10\%$) in these samples, as
297 reported in Table 1.

298

299 **3.4 Radiocarbon dating of travertines**

300 All ^{14}C ages of preserved travertines were determined at the National Ocean
301 Sciences Accelerator Mass Spectrometry Facility (NOSAMS) at Woods Hole

302 Oceanographic Institution, including data reported in previous studies and new ages
303 obtained for this study. Most of the ^{14}C ages reported in Table 1 were obtained by
304 Mervine et al. (2014), and detailed methods are reported in that publication. Additional
305 ^{14}C ages were obtained on recent travertine samples OM07-34C and OM08-200 in 2008
306 and reported in Kelemen et al. (2011). Two travertine terrace subsamples previously
307 analyzed by Mervine et al. (2014), OM10-32C-8 and OM10-32C-10, were submitted to
308 NOSAMS for re-analysis in 2014, and these new data are reported in Table 1. All ^{14}C
309 data were corrected for isotopic fractionation using $\delta^{13}\text{C}$ values measured on the
310 accelerator. ^{14}C ages were calculated using 5568 years as the half-life and converted to
311 calibrated ages using the Calib 7.1 Program with the IntCal13 calibration curve (Reimer
312 et al., 2013). Because alkaline spring water emerges with essentially no dissolved carbon
313 and most carbonates form from direct uptake of atmospheric CO_2 , no correction for the
314 possible effects of dead carbon is made in the calculation of ^{14}C ages (Mervine et al.,
315 2014).

316

317 **3.5 Stable isotope measurements of carbonates**

318 *3.5.1 Carbon and oxygen isotope measurement*

319 Stable carbon and oxygen isotope compositions were determined for all carbonate
320 samples. $\delta^{13}\text{C}$ and $\delta^{18}\text{O}$ data for fresh carbonate precipitates collected along alkaline
321 spring flow paths at Falajj and Al Bana travertine sites in 2012 were obtained in the
322 Environmental Isotopes Laboratory at the University of Waterloo using a GVI IsoPrime
323 continuous flow isotope ratio mass spectrometer system (CF-IRMS) following automated
324 phosphoric acid digestion at 90°C . The external precisions for these measurements are

325 $\pm 0.2\%$ (1 S.D.) for $\delta^{18}\text{O}$ and $\pm 0.1\%$ (1 S.D.) for $\delta^{13}\text{C}$. Bulk stable isotopic data ($\delta^{13}\text{C}$ and
326 $\delta^{18}\text{O}$) for two of these samples and all other carbonate samples were obtained at Woods
327 Hole Oceanographic Institution simultaneously with Δ_{47} , as part of the clumped isotope
328 measurement, and were normalized by reference to the carbonate standard NBS-19
329 analyzed in each analytical session, with precisions of $\pm 0.08\%$ and $\pm 0.10\%$ (1 S.D.)
330 respectively. All the carbonate isotope values are reported relative to Vienna Pee-Dee
331 Belemnite (VPDB) in Table 3.

332

333 *3.5.2 Clumped isotope measurement: Method*

334 Clumped isotope analyses were performed at Woods Hole Oceanographic
335 Institution on a Thermo MAT-253 stable isotope mass spectrometer coupled to an
336 automated sample digestion and purification line (Thornalley et al., 2015; Spooner et al.,
337 2016). For each carbonate measurement, 3-5 mg of powdered sample material are loaded
338 into silver capsules for in vacuo digestion in a common acid bath of 103% phosphoric
339 acid ($\rho = 1.92 \text{ g/cm}^3$) at 90°C for 20 minutes. During this reaction, evolved CO_2 is
340 continuously frozen into a trap immersed in a dewar of liquid nitrogen (LN2), after
341 passing through a cryogenic trap maintained at -78°C . Upon completion of the acid
342 digestion step, the collection trap is warmed to -78°C , and the CO_2 is transported by a He
343 carrier gas at a controlled flow rate of 30 ml/minute through a custom-made 60 cm long
344 gas chromatography (GC) column (Porapak Q, 50-80 mesh) held at -20°C before being
345 collected in a second LN2 trap. After the He carrier gas is pumped away, the purified
346 CO_2 is again warmed to -78°C and transferred to a small glass LN2 trap. The CO_2 is then
347 allowed to expand into the sample bellow of the mass spectrometer. All gas standards

348 (i.e. heated gases and equilibrated gases; see section 3.5.3) used in the construction of the
349 absolute reference frame are introduced and purified in the same manner as CO₂ derived
350 from carbonate samples: passing through a -78°C trap and allowed to collect in a LN₂
351 trap for 20 minutes before further GC and cryogenic purification. Purified CO₂ were
352 measured against a bottle of working reference CO₂ (Oztech CO₂, $\delta^{18}\text{O}_{\text{VSMOW}} = 25.04\text{‰}$,
353 $\delta^{13}\text{C}_{\text{VPDB}} = -3.63\text{‰}$) at a bellow pressure resulting in a signal of 12V on mass-44. Each
354 clumped isotope measurement consists of 6 acquisitions, with 9 cycles of sample-
355 reference comparison (20s of integration time) in each acquisition.

356

357 *3.5.3 Clumped isotope measurement: Data reduction*

358 Carbonate samples were analyzed over the course of three analytical sessions
359 (January-February, March-April, and July 2014), with each sample analyzed 3-8 times.
360 Four measurements from the first analytical session were excluded from the final sample
361 averages because $\delta^{13}\text{C}$ and $\delta^{18}\text{O}$ values were several permil higher than other replicate
362 measurements and/or Δ_{47} values differed significantly (up to 0.11‰) from other replicate
363 measurements. These discrepancies were due to variations in the He carrier gas flow rate
364 prior to installation of a mass flow controller. As a result, only two replicates are included
365 in the averages for two of the travertine samples because insufficient sample material
366 remained for additional replicate measurements.

367 Pure CO₂ gases of different bulk isotope compositions equilibrated at 1000°C and
368 25°C or 40°C (commonly referred to as ‘heated gases’ and ‘equilibrated gases’) were
369 analyzed on a daily basis during all three analytical sessions, to correct for instrument
370 nonlinearities and to construct the absolute reference frame (Huntington et al., 2009;

371 Dennis et al., 2011). For heated gases, aliquots of CO₂, including isotopically depleted
372 CO₂ derived from Oman travertine sample OM07-34C, were sealed in quartz tubes and
373 heated in a muffle furnace set at 1000°C for at least 1 hour. Equilibrated gases consisted
374 of CO₂ equilibrated with water maintained at either 40°C prior to May 2014 (sessions 1
375 and 2) or 25°C subsequently (session 3). Two in-house carbonate standards, NBS-19 and
376 102-GC-AZ01, were also analyzed on a nearly daily basis to monitor system stability
377 within each analytical session and to evaluate potential inter-laboratory differences in
378 clumped isotope measurements.

379 Carbonate clumped isotope data from these sessions were projected into the
380 absolute reference frame of Dennis et al. (2011), based on the heated and equilibrated
381 gases analyzed during a given session (See Supplementary Table S1 for heated and
382 equilibrated gas analyses, slopes, and intercepts for each session). During the first
383 analytical session, the flow rate of the He carrier gas during the GC purification step
384 occasionally drifted to lower values (e.g., 24 ml/min instead of 30 ml/min). This resulted
385 in significantly higher measured values of $\delta^{13}\text{C}$, $\delta^{18}\text{O}$, and Δ_{47} for some heated gas and
386 carbonate analyses. These data were excluded from the construction of the gas reference
387 frame for this session, but are still reported in Supplementary Table S1 for reference.
388 Addition of a mass flow controller to maintain the He flow at 30 ± 1 ml/min eliminated
389 this problem in subsequent analytical sessions. By convention, carbonate Δ_{47} values are
390 normalized to acid digestions performed at 25°C by addition of an acid digestion
391 correction factor. We use an acid digestion correction factor of 0.092‰, determined by
392 Henkes et al. (2013) where the analytical setup was very similar to that used for our
393 analyses at WHOI.

394 Measurements of two in-house carbonate standards in the three analytical sessions
395 yielded Δ_{47} values of $0.391 \pm 0.019\text{‰}$ (1 S.D., $n=8$), $0.422 \pm 0.021\text{‰}$ ($n=17$) and $0.424 \pm$
396 0.016‰ ($n=12$) for NBS19, and $0.725 \pm 0.018\text{‰}$ ($n=28$), $0.737 \pm 0.020\text{‰}$ ($n=30$) and
397 $0.733 \pm 0.024\text{‰}$ ($n=13$) for 102-GC-AZ01, respectively. These values are either within or
398 close to the range of the average values reported in a recent inter-laboratory study, 0.392
399 $\pm 0.017\text{‰}$ (1 S.D.) for NBS19 and $0.713 \pm 0.12\text{‰}$ (1 S.D.) for 102-GC-AZ01 (Dennis et
400 al., 2011). The inter-laboratory difference in clumped isotope measurements is currently a
401 subject of extensive investigation in the clumped isotope community, and is suspected to
402 be related to the difference in the exact analytical protocols in different laboratories (e.g.,
403 during the acid digestion process, Came et al. 2014; Defliese et al. 2015).

404 To account for these inter-laboratory difference in clumped isotope
405 measurements, we applied an additional correction to our clumped isotope data in this
406 study, based on a linear function required to bring these carbonate standards' clumped
407 isotope values in each session into agreement with their previously reported values
408 (Spooner et al. 2016). This approach is similar to the method Dennis et al. (2011)
409 outlined for constructing a secondary reference frame based on carbonate standards. The
410 robustness of this correction procedure has been evaluated in a recent inter-laboratory
411 comparison exercise between the WHOI and Caltech laboratories, where the same
412 powdered carbonate samples were distributed and analyzed at both labs (Spooner et al.,
413 2016). Excellent agreement was observed between the two labs, when the WHOI data
414 were corrected based on the reported Δ_{47} values for NBS19 and 102-GC-AZ01 obtained
415 at Caltech (0.392‰ and 0.724‰ respectively; Dennis et al., 2011; Spooner et al., 2016).
416 We adopt the same reported Δ_{47} values for these two standards during the data correction

417 in this study. Note, the magnitude of this additional correction, an average of 0.005‰ and
418 up to a maximum of 0.015‰, is over one order of magnitude smaller than the range of
419 Δ_{47} variations observed in our carbonate samples (0.21‰; see section 4.3.2), and thus it
420 should not affect the conclusion of this study.

421

422 **4. Results**

423 **4.1 Alkaline spring conditions**

424 Physiochemical conditions of the alkaline spring water, including temperature,
425 pH, $\delta^{18}\text{O}_{\text{water}}$, δD , $\delta^{13}\text{C}_{\text{DIC}}$, and concentrations of DIC, Mg^{2+} , and Ca^{2+} , are reported in
426 Table 2 and plotted in Figures 3 and 4 and Supplementary Figures S1 and S2.

427 Spring water temperatures and pH values measured in this study range from 21.7
428 to 32°C and from 11.2 to 12.1, falling within the temperature and pH ranges previously
429 reported for hyperalkaline springs in Oman (i.e., 17-39°C and 11.0-12.0 for hyperalkaline
430 springs that have not mixed with wadi water; Neal and Stanger, 1985; Paukert et al.,
431 2012; Chavagnac et al., 2013b). The subset of these measurements that were made at the
432 time of collection of fresh carbonate precipitates range from 22.5 to 28.7°C and from
433 11.2 to 11.6. Some springs were sampled in the same location in multiple years,
434 demonstrating inter-annual variability up to 4.2°C and 0.4 pH units (see samples from the
435 same “Site” in Table 2). All the water samples analyzed in this study were collected in
436 January, but seasonal variations in the spring water temperature and pH observed in
437 previous studies were small. For example, year-round observations of one hyperalkaline
438 spring yielded temperatures of 31-36°C and pH of 11.4 to 11.8 with the exception of rare
439 influxes of fresh surface waters (Neal and Stanger, 1985). Note that carbonate

440 precipitation may also occur where alkaline spring waters mix with wadi (stream) waters,
441 yielding pH values between 9 and 11 (Paukert et al., 2012; Chavagnac et al., 2013a), but
442 only one of the fresh carbonate precipitates we analyzed (OM11_07Y) was formed at
443 such a location (“Misbit mixing”) with a pH of 10.6 (Table 2).

444 $\delta^{18}\text{O}_{\text{water}}$ values of hyperalkaline springs measured in this study range from -1.5‰
445 to 2.5‰ VSMOW, with an average of 0.1 ± 1.0 ‰ VSMOW (1 S.D.), consistent with
446 previously published oxygen isotope compositions of hyperalkaline springs in Oman
447 (e.g., average of -1.1 ± 0.8 ‰ VSMOW (1 S.D.); Neal and Stanger, 1985). $\delta\text{D}_{\text{water}}$ values
448 of hyperalkaline springs measured in this study range from -8.5‰ to 9.8‰ VSMOW and
449 are strongly correlated with $\delta^{18}\text{O}_{\text{water}}$. The isotopic compositions of spring waters lie
450 below the global meteoric water line (GMWL), suggesting evolution along evaporative
451 trends (Figure 3, Craig, 1961). $\delta^{13}\text{C}_{\text{DIC}}$ values in hyperalkaline springs range from -
452 28.7‰ to -6.0‰ VPDB, with an average of -17.6 ± 4.8 ‰ (1 S.D.). Inter-annual
453 variability of the isotopic composition of water at individual springs is smaller than the
454 variability between different springs. $\delta^{18}\text{O}_{\text{water}}$, $\delta\text{D}_{\text{water}}$ and $\delta^{13}\text{C}_{\text{DIC}}$ values measured in the
455 same pools in different years differ from one another by 0.1 to 1.7‰, 1.1‰ to 7.4‰ and
456 0.04‰ to 9.2‰, respectively (Table 2).

457 The chemical and isotopic composition of water samples collected along flow
458 paths emanating from a single alkaline source spring and traveling in shallow flows along
459 the surface of travertine terraces exhibit some characteristics indicating combined effects
460 of progressive evaporation, CO_2 uptake, and carbonate precipitation, but there are no
461 systematic trends common to all flow paths (Figure 4, Figure S2). For example, $\delta^{18}\text{O}_{\text{water}}$
462 and $\delta\text{D}_{\text{water}}$ are strongly correlated and increase along evaporative trends for some flow

463 paths. pH also decreases with greater distance from the source spring, as would be
464 expected during CO₂ uptake or carbonate precipitation, for some but not all flow paths
465 (Figure S2). Similarly, for the two flow paths where DIC concentration data are available,
466 DIC concentration increases slightly overall along the flow paths. Ca concentration
467 generally decreases along the flow path, as would be expected with precipitation of
468 calcium carbonate. Mg concentration remains constant, or increases for flow paths where
469 correlated increases in $\delta^{18}\text{O}_{\text{water}}$ and $\delta\text{D}_{\text{water}}$ suggest progressive evaporation (Figure S2).

470

471 **4.2 Carbonate mineralogy and ¹⁴C ages**

472 Carbonate minerals identified by XRD and Raman spectroscopy analysis are
473 presented in Table 1. Fresh precipitates in this study are composed of pure calcite, pure
474 aragonite, and mixtures of calcite and aragonite, with calcite more common in crusts
475 formed at pool surfaces and aragonite more common in fine precipitates found lining
476 alkaline pools and spring outlets. This distribution of calcite and aragonite is consistent
477 with the mineralogy observed in other hyperalkaline springs in Oman (Chavagnac et al.,
478 2013a). In contrast, preserved travertines are predominantly calcite, with minor amounts
479 of aragonite found only in one recently-formed travertine sample (OM09-89C).

480 The calibrated ¹⁴C ages of fresh carbonate precipitates and of travertine deposits
481 considered in this study, range from modern to 350 years and from modern to 45,000
482 years, respectively, where “modern” is defined by >95% of the ¹⁴C activity for AD 1950
483 (Olsson, 1970; Kelemen and Matter, 2008; Kelemen et al., 2011; Mervine et al., 2014;
484 this study). Two of the travertine subsamples (OM10-32C-8 and OM10-32C-10) dated by
485 Mervine et al. (2014) were re-analyzed in this study, yielding calibrated ¹⁴C ages of

486 18,350 ± 118 (1 S.D.) years and 15,640 ± 126 years, respectively. These ages are
487 different from their previously reported calibrated ¹⁴C ages (16,710 ± 133 years and
488 23,710 ± 215, respectively; Mervine et al., 2014), which could be related to heterogeneity
489 of the travertine samples. Because the ¹⁴C analyses in this study were performed on the
490 same aliquots of sample powders used in the clumped isotope analyses, we refer to these
491 ¹⁴C ages in Table 1 and in the following discussion.

492

493 **4.3 Stable isotope compositions of carbonates**

494 We present the results of stable isotope analyses ($\delta^{13}\text{C}$, $\delta^{18}\text{O}$ and Δ_{47}) of fresh
495 carbonate precipitates and preserved travertines in Table 3. Raw data of the clumped
496 isotope analyses, including all analyses of samples, carbonate standards, heated gases,
497 and equilibrated gases, are reported in Supplementary Table S1.

498

499 *4.3.1 Oxygen and carbon isotope compositions*

500 $\delta^{18}\text{O}$ and $\delta^{13}\text{C}$ values of fresh carbonate precipitates and preserved travertines range
501 from highly depleted values (e.g., $\delta^{18}\text{O}_{\text{VPDB}}$ and $\delta^{13}\text{C}_{\text{VPDB}}$ as low as -16.9‰ and -27.2‰
502 respectively) to values approaching expected equilibrium with spring waters (e.g.,
503 $\delta^{18}\text{O}_{\text{VPDB}} = 0\text{‰}$ and $\delta^{13}\text{C}_{\text{VPDB}} = -4\text{‰}$), with a strong positive correlation between the two
504 (overall $\delta^{13}\text{C}$ vs. $\delta^{18}\text{O}$ slope of 1.1, $R^2=0.83$; Figure 5a). The $\delta^{18}\text{O}$ and $\delta^{13}\text{C}$ values
505 recorded in these samples overlap with that observed in previous studies of Oman
506 travertine (-17 to +6‰ in $\delta^{18}\text{O}$, -33 to +3‰ in $\delta^{13}\text{C}$, and $\delta^{13}\text{C}$ vs. $\delta^{18}\text{O}$ slope of 1.3, Clark
507 and Fontes, 1990; Clark et al., 1992; Kelemen et al., 2011; Mervine et al., 2014). The
508 bulk oxygen and carbon isotopic compositions of fresh carbonate precipitate samples

509 collected in 2009-2010 and all of the preserved travertine samples in this study were also
510 analyzed in previous studies. $\delta^{13}\text{C}$ and $\delta^{18}\text{O}$ derived from our clumped isotope analyses
511 typically fall within 0.3‰ of the previously reported values (Supplementary Figure S3;
512 Kelemen et al., 2011; Mervine et al., 2014). Greater differences were observed between
513 the isotopic compositions derived from clumped isotope analyses at WHOI and those
514 measured at the University of Waterloo: for the two samples analyzed in both
515 laboratories, measurements made at WHOI were 1.48‰ lower in $\delta^{13}\text{C}$ and 0.50‰ higher
516 in $\delta^{18}\text{O}$ for OM12_07V and 4.28‰ higher in $\delta^{13}\text{C}$ and 0.95‰ lower in $\delta^{18}\text{O}$ for
517 OM12_07X2. The source of this discrepancy is unknown, but it suggests that caution
518 should be taken in interpreting small variations in the stable isotope compositions of fresh
519 carbonates along alkaline spring flow paths measured at the University of Waterloo.
520 Regardless, these differences remain small relative to the range of isotopic compositions
521 observed in carbonates formed at hyperalkaline springs in Oman.

522 The most depleted $\delta^{18}\text{O}$ and $\delta^{13}\text{C}$ values are observed in fresh carbonate films on
523 alkaline spring surfaces and in recently-formed preserved travertines (pale blue diamonds
524 and green squares in Figure 5a), but several bottom floc samples also record highly
525 depleted bulk isotopic compositions (dark blue diamonds in Figure 5a). Isotopic
526 depletions are not restricted only to recently-formed samples. Even travertines as old as
527 40,000 years may preserve significantly depleted isotopic values, e.g., $\delta^{18}\text{O}_{\text{VPDB}} \sim -13\text{‰}$
528 and $\delta^{13}\text{C}_{\text{VPDB}} \sim -20\text{‰}$.

529 Samples at the equilibrium end of the observed $\delta^{13}\text{C}$ - $\delta^{18}\text{O}$ trend consist of several old
530 travertines and a few bottom flocs that line hyperalkaline pools. Their isotopic
531 compositions appear to be in equilibrium with the observed range of present-day spring-

532 water temperatures and $\delta^{18}\text{O}$ values and with the carbon isotope composition of soil or
533 atmospheric CO_2 (Table 2 and 4; Neal and Stanger, 1985; Clark et al., 1992; Matter,
534 2005). Bottom floc samples exhibit slightly lower $\delta^{13}\text{C}$ than the older travertines and are
535 thus closer to the expected equilibrium with vegetation-influenced soil CO_2 than
536 atmospheric CO_2 (Clark and Fontes, 1990; Clark et al., 1992). Note however, caution
537 should be taken when interpreting the isotopic composition of older travertines in the
538 context of the present-day conditions in Oman. Although conditions similar to today may
539 have prevailed during many periods in the past, both temperature and $\delta^{18}\text{O}$ of meteoric
540 water have varied in Oman over the past 50,000 years (e.g., Burns et al., 2001;
541 Weyhenmeyer et al., 2000). Thus, older travertine samples that appear to be in
542 equilibrium with present-day spring-water conditions could have formed in equilibrium at
543 times when temperature and stable isotope compositions of water were similar to those
544 observed today, or these samples may have formed under isotopic disequilibrium but re-
545 equilibrated isotopically with similar conditions at a later time.

546 There appears to be a weak correlation between the mineralogy and stable isotope
547 composition in fresh carbonate precipitates, with calcite more abundant in highly
548 fractionated samples and aragonite more abundant in the samples whose isotopic
549 compositions are closer to isotopic equilibrium. The average $\delta^{18}\text{O}$ value of fresh
550 carbonate precipitates composed of >90% aragonite (n=3) is only ~2‰ lower than
551 expected equilibrium values for average spring conditions of $T=28 \pm 4^\circ\text{C}$, $\delta^{18}\text{O}_{\text{water}}=0.1$
552 ± 1.0 ‰ SMOW (1 S.D.), while the average $\delta^{18}\text{O}$ value of fresh carbonate precipitates
553 composed of >90% calcite (n=3) is ~12‰ lower than expected equilibrium values for
554 these average spring conditions (Kim and O'Neil, 1997; Kim et al., 2007). The average

555 $\delta^{18}\text{O}$ value of fresh carbonate precipitates composed of mixtures of both calcite and
556 aragonite (at least ~20% of each, n=8) is ~8-9‰ lower than expected equilibrium values
557 for these average spring conditions, but mixed samples with higher proportions of calcite
558 do not always have larger deviations from equilibrium.

559

560 *4.3.2 Clumped isotope compositions*

561 Similar to their bulk $\delta^{18}\text{O}$ and $\delta^{13}\text{C}$ values, Δ_{47} values in fresh carbonate
562 precipitates and preserved travertines also vary significantly, ranging from enriched
563 values (as high as 0.883‰) to values approaching equilibrium with observed alkaline
564 spring temperatures (e.g., observed Δ_{47} as low as 0.750‰ in fresh precipitates and
565 0.675‰ in preserved travertines compared to expected equilibrium Δ_{47} values of 0.65-
566 0.75‰ for 17-39 °C; Ghosh et al., 2006; Dennis et al., 2011). The magnitude of Δ_{47}
567 enrichments observed in our samples, ~0.13-0.23‰ relative to the expected equilibrium,
568 are similar to those observed in carbonates derived from high-pH laboratory precipitation
569 experiments (~0.12-0.25‰, Schmid, 2011; ~0.26-0.31‰, Tang et al., 2014) and in
570 travertines from hyperalkaline springs in Liguria (~0.19-0.24‰, Schmid, 2011).

571 We note inter-laboratory difference exists in the calibration of clumped isotope
572 thermometers (e.g., Ghosh et al., 2006; Dennis and Schrag, 2010; Zaarur et al., 2013;
573 Defliese et al., 2015; Kluge et al., 2015). In this study, we discuss our results by reference
574 to the equilibrium clumped isotope values predicted by the calibration of Ghosh et al.
575 (2006) as re-calculated in the absolute reference frame by Dennis et al. (2011). We regard
576 this as the most appropriate calibration for our data at this stage because our data have
577 been normalized to the accepted values of the two in-house carbonate standards at

578 Caltech (section 3.5.3). High Δ_{47} materials yield higher Δ_{47} values when analyzed at
579 Caltech than in many other labs (Dennis et al., 2011), consistent with the steepness of the
580 Ghosh et al. (2006) calibration produced at Caltech, which appears to remain valid for a
581 wide variety materials analyzed at Caltech regardless of updated digestion procedures at
582 90°C (Falk and Kelemen, 2015; Tripathi et al., 2015). We therefore consider consistent
583 standard measurements to be a more important factor in choosing an appropriate clumped
584 isotope calibration to apply than acid digestion temperature. More importantly, over the
585 temperature range of spring water in Oman (17-39°C), the expected equilibrium Δ_{47}
586 values are similar for other existing carbonate clumped isotope calibrations (e.g., Dennis
587 and Schrag, 2010; Zaarur et al., 2013; Defliese et al., 2015; Kluge et al., 2015). The
588 maximum difference in expected equilibrium Δ_{47} values derived from different
589 calibrations is $\sim 0.03\text{‰}$, much smaller than the range of Δ_{47} variations observed in our
590 samples. Therefore, the choice of clumped isotope equilibrium calibration should not
591 affect the conclusion of this study.

592 Relative to expected equilibrium values at average ambient temperatures and fluid
593 isotopic compositions ($\delta^{18}\text{O}_{\text{water}} \sim 0\text{‰}$, $T \sim 28^\circ\text{C}$; Table 2), enrichments in Δ_{47} in fresh
594 carbonate precipitates correlate with depletions in their $\delta^{13}\text{C}$ and $\delta^{18}\text{O}$, yielding a Δ_{47} -
595 $\delta^{18}\text{O}$ slope of -0.011 between samples furthest from isotopic equilibrium and expected
596 equilibrium values (Figure 5). Crystalline films from alkaline pool surfaces, which show
597 the largest depletions in $\delta^{13}\text{C}$ and $\delta^{18}\text{O}$, record enriched Δ_{47} values of $0.85 \pm 0.01\text{‰}$
598 (Figure 5b), about 0.10-0.20‰ higher than expected for the range of temperatures
599 observed in alkaline springs in Oman ($\sim 17\text{-}39^\circ\text{C}$; Table 2; Paukert et al., 2012;
600 Chavagnac et al., 2013b). These Δ_{47} values correspond to unrealistically low apparent

601 clumped isotope temperatures of $\sim 0^\circ\text{C}$ (Ghosh et al., 2006; Dennis et al., 2011). Similar
602 disequilibrium isotopic signatures are also observed in some bottom floc samples, with
603 enriched Δ_{47} values of 0.773-0.883‰. In contrast, aragonite-rich bottom floc whose ^{13}C
604 and ^{18}O fall within the range of expected equilibrium values for ambient conditions in
605 Oman record Δ_{47} values of 0.738-0.758‰ (Figure 5b), corresponding to apparent
606 clumped isotope temperatures of $17\text{-}13^\circ\text{C}$ (Ghosh et al., 2006; Dennis et al., 2011). These
607 apparent temperatures are slightly lower than the lowest spring temperatures measured
608 during the winter field seasons, but are consistent with typical winter air temperatures in
609 Oman (Paukert et al., 2012; Oman Directorate General of Meteorology, 2015).

610 Clumped isotope compositions of preserved travertines also span a large range of
611 Δ_{47} values, from 0.855‰ to 0.675‰, which correspond to apparent clumped isotope
612 temperatures of -1°C to 33°C (Figure 5c). Similar to their $\delta^{13}\text{C}$ and $\delta^{18}\text{O}$, Δ_{47} values of
613 recently-formed travertines (i.e., with calibrated ^{14}C ages between modern and 305 years)
614 overlap with those observed in fresh precipitates at the disequilibrium end of the isotopic
615 trends. Some older travertine subsamples (calibrated ^{14}C ages of 18,350 - 41,610 years)
616 also record disequilibrium $\delta^{13}\text{C}$, $\delta^{18}\text{O}$, and Δ_{47} values overlapping those observed in
617 recently-formed travertines, while other travertine subsamples (calibrated ^{14}C ages of
618 34,000-45,000 years) record $\delta^{13}\text{C}$, $\delta^{18}\text{O}$, and Δ_{47} values between the disequilibrium values
619 observed in recently-formed travertines and values consistent with equilibrium at
620 temperatures of $\sim 35^\circ\text{C}$ (Kim and O'Neil, 1997; Ghosh et al., 2006; Dennis et al., 2011).
621 Note that some subsampled layers in one travertine outcrop (OM10-32) yield Δ_{47} values
622 higher than expected from the isotopic trends observed in fresh precipitates. These

623 additional enrichments are interpreted to reflect mixing between isotopically distinct
624 generations of carbonate within the travertine layers (see discussion in section 5.1.3).

625

626 **5. Discussion**

627 **5.1 Fresh calcium carbonate precipitates**

628 *5.1.1 Disequilibrium end-member*

629 Among different types of fresh carbonate precipitates, surface films record the
630 greatest extent of stable isotope disequilibrium (e.g., $\delta^{18}\text{O}_{\text{VPDB}} = -16.7\text{‰}$, $\delta^{13}\text{C}_{\text{VPDB}} = -$
631 27.2‰ , $\Delta_{47} = 0.851\text{‰}$), but several bottom flocc samples from shallow flow paths along
632 travertine surfaces also fall close to this end-member. Note, some of these bottom flocc
633 samples may have formed initially as surface films and then settled to the bottom rather
634 than precipitating *in situ*.

635 Under the high pH conditions observed in alkaline springs, CO_2 uptake and carbonate
636 precipitation is very rapid at the air-water interface. O'Neil and Barnes (1971) proposed
637 that depleted $\delta^{13}\text{C}$ and $\delta^{18}\text{O}$ values in travertines from alkaline springs in northern
638 California result from CO_2 diffusion kinetics across the air-water interface. However,
639 Clark et al. (1992) found this mechanism could not fully explain the kinetic isotope
640 effects observed in their high-pH carbonate precipitation experiments and suggested
641 instead that the observed depletions in $\delta^{13}\text{C}$ and $\delta^{18}\text{O}$ in alkaline spring carbonates are
642 related to the CO_2 hydroxylation reaction. They concluded that depleted $\delta^{13}\text{C}$ values in
643 these carbonates were best explained by a kinetic isotope fractionation on the order of
644 15‰ during hydroxylation, while their depleted $\delta^{18}\text{O}$ values resulted from unidirectional
645 reaction of CO_2 with hydroxyl ions, which are isotopically lighter than H_2O molecules by

646 ~ 40‰ (Green and Taube, 1963). This mechanism was supported by studies of calcite
647 precipitation from high pH solutions (e.g., pH>12, Dietzel et al., 1992; Kosednar-
648 Legenstein et al., 2008), and their estimated carbon isotope fractionation fall within the
649 range from other experimental studies (e.g., 11 to 39‰ over 18-24°C, Zeebe and Wolf-
650 Gladrow, 2001).

651 Strong depletions in $\delta^{13}\text{C}$ and $\delta^{18}\text{O}$ of the surface film samples are accompanied by
652 significant enrichments in their Δ_{47} values. Although the exact mechanism generating
653 these Δ_{47} enrichments cannot be determined from these data alone, it is expected that the
654 CO_2 hydroxylation reaction responsible for depletions in their $\delta^{13}\text{C}$ and $\delta^{18}\text{O}$ will also
655 produce kinetic enrichments in their clumped isotope compositions (Appendix A). We
656 obtain a first-order estimate on the clumped isotope composition of the HCO_3^- produced
657 from the CO_2 hydroxylation reaction, assuming isotopic composition of the CO_2 is in
658 equilibrium with water and no kinetic isotope fractionation is associated with CO_2
659 hydroxylation (i.e. random addition of OH^-). Similar assumptions have been employed in
660 previous studies to estimate the oxygen isotope composition of the HCO_3^- derived from
661 this reaction (e.g., Rollion-Bard et al., 2003). Our estimation suggests that, at 300K, CO_2
662 hydroxylation leads to enriched clumped isotope compositions of HCO_3^- relative to the
663 expected equilibrium values, with a Δ_{47} - $\delta^{18}\text{O}$ slope of -0.012 (See details in Appendix A).

664 Because CO_2 uptake and carbonate precipitation is rapid at the air-water interface in
665 alkaline springs, there are limited opportunities for oxygen isotope and clumped isotope
666 equilibration of the DIC, especially under those high pH conditions. Therefore, the Δ_{47}
667 values of the carbonates precipitated at the surface of alkaline springs are expected to
668 reflect that of the HCO_3^- derived from the CO_2 hydroxylation reaction and be enriched

669 relative to the expected equilibrium values. The agreement between our theoretically
670 estimated Δ_{47} - $\delta^{18}\text{O}$ slope of -0.012 and the Δ_{47} - $\delta^{18}\text{O}$ slope of -0.011 observed between
671 surface film samples and values expected in equilibrium with average spring water
672 conditions ($\delta^{18}\text{O}_{\text{water}} \sim 0\text{‰}$, $T \sim 28^\circ\text{C}$; Table 2) further supports CO_2 hydroxylation as the
673 main cause of the observed depletions in $\delta^{18}\text{O}$ and $\delta^{13}\text{C}$ and enrichments in Δ_{47} (Figure
674 5).

675

676 *5.1.2 Equilibrium end-member*

677 The $\delta^{13}\text{C}$, $\delta^{18}\text{O}$, and Δ_{47} values of some bottom floc samples are close to the
678 equilibrium values expected for conditions observed in Oman alkaline springs and
679 surface runoff waters. The bottom floc samples with isotopic compositions closest to
680 expected equilibrium values are rich in aragonite. However, calcite and aragonite cannot
681 be strictly assigned as disequilibrium and equilibrium end-members respectively because
682 some surface film samples recording strong disequilibrium isotopic signatures also
683 contain significant proportions of aragonite. Instead, we suggest that aragonite
684 precipitation may be favored relative to calcite under conditions where isotopic
685 equilibrium is also more likely to be achieved.

686 Chavagnac et al. (2013a) suggest aragonite precipitation may be favored when
687 surface runoff, containing much higher concentrations of Mg^{2+} and DIC than alkaline
688 spring water, reacts with alkaline spring water. This could occur either as surface runoff
689 enters an alkaline pool or when alkaline spring waters seep back into pools that have been
690 flooded with surface runoff. Increases in the Mg/Ca ratio under these conditions could
691 favor precipitation of aragonite rather than calcite, and atmospheric- or soil-derived DIC

692 in the surface runoff could have already equilibrated isotopically before reaction with
693 alkaline fluids, leading to apparent equilibrium values in $\delta^{13}\text{C}$, $\delta^{18}\text{O}$, and Δ_{47} of the
694 resulting bottom floc. Thus, the isotopic composition of bottom floc samples that appear
695 close to equilibrium could reflect conditions during infrequent surface runoff events (i.e.,
696 rainy days) rather than the observed alkaline spring conditions.

697 It is however important to note that bottom floc samples could represent mixtures of
698 carbonates formed at different times under varying conditions. They may comprise
699 carbonate precipitated at the bottom of the pool, surface films that have broken and
700 settled to the bottom, or carbonate terraces formed on the edge of the pool that have
701 slumped or been washed into the pool. It is also unknown how long these samples have
702 remained at the bottom of the pool before they were collected. Thus, while we can be
703 fairly certain that surface films formed under the observed conditions at the surface of the
704 pools, the conditions at the time of bottom floc precipitation are not necessarily the same
705 as the conditions measured in the alkaline springs at the time of sample collection.

706

707 *5.1.3 Mixing between disequilibrium and equilibrium end-members*

708 We note that some bottom floc samples with $\delta^{13}\text{C}$ and $\delta^{18}\text{O}$ compositions
709 intermediate between the most kinetically fractionated values and equilibrium values
710 have Δ_{47} values in excess of linear trends between the enriched disequilibrium values
711 observed in surface films and values representing equilibrium with observed water
712 temperatures (Figure 6). This suggests that some bottom floc samples, particularly those
713 formed in larger alkaline pools, may represent mixtures between these two isotopically
714 distinct carbonate end-members.

715 It is known that mixing of two carbonates with different $\delta^{13}\text{C}$ and $\delta^{18}\text{O}$ may result in a
716 Δ_{47} value of the mixture that is not linear with respect to the proportions of the two end-
717 members (Eiler and Schauble, 2004; Affek and Eiler, 2006; Halevy et al., 2011, Defliese
718 and Lohmann, 2015). The exact Δ_{47} value of the mixture can be higher or lower than the
719 weighted average of the two end-members, depending on the differences in the $\delta^{13}\text{C}$ and
720 $\delta^{18}\text{O}$ of the two end-members. For two end-members whose $\delta^{13}\text{C}$ and $\delta^{18}\text{O}$ values are
721 positively correlated, as in carbonates precipitated at alkaline springs, mixing is expected
722 to lead to a positive Δ_{47} anomaly that is a quadratic function of the mixing ratio and
723 whose magnitude increases with the difference in bulk stable isotope compositions
724 between end-members.

725 We therefore calculate the expected clumped isotope compositions for mixing
726 between the disequilibrium end-member and several possible equilibrium end-members
727 covering the observed ranges of temperatures in northern Oman, $\delta^{18}\text{O}_{\text{water}}$ of alkaline
728 spring waters, and $\delta^{13}\text{C}$ of soil or atmospheric CO_2 (Figure 6, Table 4). These
729 calculations show that the bulk stable isotope and clumped isotope compositions of most
730 bottom floc samples from larger alkaline pools (open blue diamonds in Figure 6) are not
731 consistent with mixing with an end-member that formed under equilibrium with alkaline
732 spring conditions observed at the time of collection. For example, the “Misbit” curve in
733 Figure 6 does not pass through precipitates collected in that spring (black crosses).
734 Instead, their isotopic compositions are better explained by mixing between the
735 disequilibrium end-member and an equilibrium end-member formed at temperatures of
736 about 17-25°C and $\delta^{13}\text{C}$ of soil CO_2 (Figure 6). While slightly lower than temperatures
737 typically observed in hyperalkaline spring water in Oman, the temperature of this inferred

738 equilibrium end-member agrees well with average winter air temperatures in northern
739 Oman (e.g., January average daily temperature range of 12-26°C in Nizwa, Oman
740 Directorate General of Meteorology, 2015), and may reflect the temperature of surface
741 runoff from winter rainfall rather than the temperature of groundwater discharge.
742 Northern Oman currently receives most of its rainfall during the winter months. The
743 agreement of average rainy season temperatures with temperatures of the inferred
744 equilibrium end-members suggests that identifying such equilibrium end-members in old
745 travertines formed in similar environments could help constrain the rainy season
746 temperatures in the past.

747 Note, one aragonite-bearing sample from the bottom of a large alkaline pool in
748 Wadi Sudari (OM09-8COPS) does not fall on the mixing trend of a low-temperature
749 equilibrium end-member, but instead would require an equilibrium end-member formed
750 at ~40°C. While it is possible that this sample reflects a carbonate component formed in
751 isotopic equilibrium with rainwater in warmer months, it may be more likely that this
752 sample formed in a shallow flow path along travertine surfaces near the edge of the pool
753 and later washed or slumped into the pool and thus reflect processes other than carbonate
754 mixing (see discussion in section 5.1.4). The fact that a layered travertine sample
755 collected from the edge of this same pool (OM09-89C) has an isotopic composition
756 extremely close to this sample supports the latter explanation.

757

758 *5.1.4 Equilibration of DIC*

759 Isotopic variations among many of the fresh precipitates that formed in shallow
760 alkaline spring flows along travertine terraces (filled blue diamonds in Figure 6) cannot

761 be explained by mixing between the disequilibrium end-member and the low-temperature
762 equilibrium end-member described above. The isotopic composition of these samples lie
763 relatively close to the disequilibrium end-member and do not show obvious curvature in
764 their $\Delta_{47}\text{-}\delta^{13}\text{C}$ and $\Delta_{47}\text{-}\delta^{18}\text{O}$ trends. If we nevertheless seek to explain the variations in
765 isotopic compositions of these samples by invoking carbonate mixing, the equilibrium
766 end-member carbonate would need to have formed above 35°C. Although such
767 temperatures can be attained in some alkaline springs in Oman, water temperatures
768 measured at the exact collection sites of these specific samples do not exceed 29°C.
769 Furthermore, these samples were found along the bottom of rivulets and small, shallow
770 pools along the surface of travertine terraces; at these locations there is less opportunity
771 for surface runoff to collect and react with alkaline spring water to form equilibrium end-
772 members than at locations where alkaline springs form larger “blue pools” within stream
773 beds.

774 Instead, we suggest that the isotope compositions of these samples reflect partial
775 isotopic equilibration of DIC in alkaline pools and surface flows, creating apparent linear
776 $\Delta_{47}\text{-}\delta^{13}\text{C}$ and $\Delta_{47}\text{-}\delta^{18}\text{O}$ trends toward the expected equilibrium values with ambient spring
777 conditions. The carbon isotope compositions of the DIC measured in the Oman alkaline
778 springs support this interpretation. $\delta^{13}\text{C}_{\text{DIC}}$ in most alkaline springs falls between -13 and
779 -20‰, rather than recording the most extreme kinetic depletions (i.e., $\delta^{13}\text{C}$ as low as -
780 27.2‰ VPDB in surface films). The lack of positive correlations between $\delta^{13}\text{C}_{\text{DIC}}$ and the
781 concentration of DIC or Mg^{2+} (Supplementary Figure S2) suggests these variations in
782 $\delta^{13}\text{C}_{\text{DIC}}$ are more likely related to gradual equilibration of initially ^{13}C -depleted DIC in
783 the alkaline pools, as opposed to mixing with surface run-off waters which would have

784 higher concentrations of DIC and Mg^{2+} and more equilibrated isotopic compositions of
785 DIC. However, we do not observe systematic shifts towards equilibrium values in the
786 isotopic compositions of DIC and carbonate precipitates along individual flow paths
787 (Figure 4). This indicates that the isotope equilibration process does not merely occur
788 incrementally along surface flow paths, but may depend also on other factors which
789 would affect the overall residence time of DIC, such as the rates of CO_2 uptake and
790 carbonate precipitation, water depth, and flow regime.

791

792 **5.2 Preserved travertines**

793 Laminated travertines with ages ranging from modern to over 40,000 years record
794 many of the same processes recorded by fresh carbonate precipitates at alkaline springs.
795 These include (1) kinetic enrichments in Δ_{47} accompanying depletions in $\delta^{13}C$ and $\delta^{18}O$,
796 associated with hydroxylation of CO_2 ; and (2) $\delta^{13}C$, $\delta^{18}O$, and Δ_{47} values that trend from
797 this kinetic disequilibrium end-member toward equilibrium values, likely reflecting
798 gradual, partial isotopic equilibration of DIC in the alkaline pools and surface flow paths.
799 However, these highly porous travertines may also be subject to continued interaction
800 with surface waters and alkaline spring waters after their original deposition, which could
801 result in additional modification of their isotopic compositions via recrystallization
802 (dissolution and re-precipitation) and/or precipitation of secondary carbonates within the
803 pore space of the travertine.

804

805 *5.2.1 Inheritance and preservation of kinetic trends*

806 The recently-formed laminated travertine samples analyzed in this study (^{14}C age
807 ≤ 305 years, $n=4$) preserve significant disequilibrium signatures in their $\delta^{13}\text{C}$, $\delta^{18}\text{O}$, and
808 Δ_{47} values (Figure 5). In these travertine samples, the variations of $\delta^{13}\text{C}$, $\delta^{18}\text{O}$, and Δ_{47}
809 away from the disequilibrium end-member are similar in slope and extent to the trends
810 attributed to partial equilibration of DIC for fresh precipitates, i.e., trends characteristic of
811 fresh precipitates formed in shallow pools and flow paths along travertine terraces.
812 Unlike fresh precipitates formed at the bottom of larger “blue pools,” none of the
813 recently-formed travertine samples record isotopic compositions close to possible
814 equilibrium values. These four samples may not be representative of all recently-formed
815 travertines and may reflect a sampling bias. Delicately layered recent travertine samples
816 were collected from exposed surfaces of travertine terraces, similar to the environment of
817 fresh precipitates formed in shallow rivulets and small pools along travertine terraces,
818 rather than larger pools within wadi (stream) beds. They are thus more closely tied to the
819 process of carbonate precipitation in shallow surface flows and crusts formed at the air-
820 water interface than to bottom flocculation in pools which are more influenced by occasional
821 surface runoff. Accordingly, we would expect their isotopic composition to reflect the
822 trends associated with kinetic disequilibrium and partial DIC equilibration rather than the
823 non-linear trends associated with mixing with isotopically equilibrated carbonate end-
824 members.

825 Several of the older travertine subsamples (20,000 – 40,000 years old) also record
826 $\delta^{13}\text{C}$, $\delta^{18}\text{O}$, and Δ_{47} values that overlap with the kinetic trends observed in fresh
827 precipitates, demonstrating that disequilibrium clumped isotope signals can be preserved

828 over these time scales and that the same processes operating in the active system today
829 are responsible for the formation of extensive fossil travertine terraces. However, the
830 $\delta^{13}\text{C}$, $\delta^{18}\text{O}$, and Δ_{47} of some older travertine subsamples extend beyond the range
831 observed in fresh precipitates and recently-formed travertines along the DIC equilibration
832 trend and closely approach the range of values expected for equilibrium with present-day
833 ambient conditions in alkaline springs. Note, $\delta^{18}\text{O}$ values of meteoric water in Northern
834 Oman may have been up to 6‰ lower than present-day values during previous
835 interglacial periods (Burns et al., 2001), and groundwater temperatures may have been
836 about 6°C cooler during the late Pleistocene (Weyhenmeyer et al., 2000). However, even
837 taking into account these variations, the isotopic compositions of these carbonate samples
838 would still appear to be close to equilibrium with paleo-conditions. We suggest isotopic
839 exchange during post-depositional recrystallization may be responsible for shifting the
840 isotopic composition of these travertine samples towards equilibrium values, as they
841 interact with surface- and ground-waters. Most fresh precipitates at alkaline springs
842 contain at least minor amounts of aragonite, but aragonite is absent from all older
843 travertine samples. This is consistent with our suggestion that recrystallization occurred
844 in these older travertine samples and has affected their isotopic compositions.

845

846 *5.2.2 Mixing with subsequent carbonate precipitates*

847 Based on their ^{14}C ages and isotopic compositions, subsampled layers (within a 1
848 m section) of travertine terrace OM10-32C can be classified into three groups: (1)
849 subsamples with calibrated ^{14}C ages of ~30 ky, whose $\delta^{13}\text{C}$ - $\delta^{18}\text{O}$ - Δ_{47} values fall on the
850 DIC equilibration trend (n=2, medium red squares in Figure 5); (2) subsamples with

851 calibrated ^{14}C ages of ~ 40 ky, whose $\delta^{13}\text{C}$ - $\delta^{18}\text{O}$ - Δ_{47} values approach equilibrium with
852 present-day ambient conditions ($n=2$, dark red squares in Figure 5); and (3) subsamples
853 with calibrated ^{14}C ages of ~ 9 -18 ky, whose $\delta^{13}\text{C}$ - $\delta^{18}\text{O}$ - Δ_{47} values deviate significantly
854 from the trends observed in fresh precipitates and recently-formed travertines ($n=3$, pink
855 squares in Figure 5). Although the linear correlation in $\delta^{13}\text{C}$ and $\delta^{18}\text{O}$ of these three
856 younger subsamples overlaps with trends in other travertine samples from this and
857 previous studies (Clark and Fontes, 1990; Clark et al., 1992; Kelemen et al., 2011;
858 Mervine et al., 2014), their enriched Δ_{47} values at intermediate $\delta^{13}\text{C}$ and $\delta^{18}\text{O}$ values are
859 strongly suggestive of mixing of two carbonate end-members. Specifically, these
860 intermediate clumped isotope compositions are consistent with mixing between travertine
861 along the DIC equilibration trend and another carbonate end-member with higher $\delta^{13}\text{C}$
862 and $\delta^{18}\text{O}$, e.g. later generations of carbonate precipitation within the pore space of the
863 travertine (Figure 7). ^{14}C data from these subsamples also support this interpretation, with
864 modern carbon fractions (F_m) positively correlating with their $\delta^{13}\text{C}$ and $\delta^{18}\text{O}$ (Figure 7b).
865 Note, mixing of travertines with a younger carbonate end-member with higher $\delta^{18}\text{O}$ could
866 generate correlations between F_m and $\delta^{18}\text{O}$, but would not necessarily form a perfect
867 linear correlation line because the travertine subsamples are unlikely to all have formed at
868 the same time.

869 Mixing between a hypothetical end-member ($\delta^{13}\text{C}_{\text{VPDB}} = 0\text{‰}$, $\delta^{18}\text{O}_{\text{VPDB}} = 3.9\text{‰}$,
870 $\Delta_{47} = 0.738\text{‰}$) and travertine lying along the DIC partial equilibration trend near the
871 isotopic composition of OM10-32C-9 ($\delta^{13}\text{C}_{\text{VPDB}} = -18.1\text{‰}$, $\delta^{18}\text{O}_{\text{VPDB}} = -10.3\text{‰}$, Δ_{47}
872 $= 0.787\text{‰}$) accurately reproduces $\delta^{13}\text{C}$, $\delta^{18}\text{O}$, Δ_{47} values of all three younger subsamples
873 of OM10-32C when the assumed proportion of the hypothetical end-member in OM10-

874 32C-8, OM10-32C-10, and OM10-32C is 8%, 43%, and 78%, respectively. This
875 hypothetical end-member was derived by extrapolating the observed $\delta^{18}\text{O}$ - $\delta^{13}\text{C}$
876 correlation in these subsamples (Figure 7a) to $\delta^{13}\text{C}_{\text{carbonate}} = 0\text{‰}$ VPDB (i.e., the
877 maximum expected equilibrium value based on ambient conditions and carbon sources;
878 Clark et al., 1992), then varying the Δ_{47} of this end-member to obtain the best fit between
879 the calculated mixing curve and the measured Δ_{47} values of the travertine subsamples
880 (Figure 7d). This hypothetical end-member is consistent with the isotopic composition of
881 a carbonate formed in isotopic equilibrium with atmospheric CO_2 ($\delta^{13}\text{C}_{\text{CO}_2} \sim -7\text{‰}$ VPDB;
882 Clark et al., 1992) and $\delta^{18}\text{O}_{\text{water}} = 5.1\text{‰}$ VSMOW at 20°C. This could represent a realistic
883 scenario where later generations of carbonates precipitate within the pore space of a
884 travertine as pore-water derived from surface waters and/or alkaline spring waters
885 evaporates.

886 Our results suggest that clumped isotope measurement can be a valuable tool for
887 identifying these kinds of mixing processes, which cannot be readily identified from bulk
888 stable isotope measurements alone. Furthermore, our results suggest measured ^{14}C ages
889 of travertine may reflect not only ages of the initial travertine formation, but also later
890 carbonate precipitation within the pore space. Depending on the age of the later carbonate
891 precipitation, the “true” ages of the above travertine subsamples can be tens of thousands
892 of years older than their measured apparent ^{14}C ages and the relative chronology of these
893 subsamples can also change substantially (see details in Appendix B).

894

895 **5.3 Summary of processes affecting isotopic compositions of carbonates associated**
896 **with alkaline springs**

897 In summary, the observed $\delta^{13}\text{C}$, $\delta^{18}\text{O}$, and Δ_{47} values in fresh carbonate
898 precipitates at alkaline springs and in preserved travertine terraces can be explained by a
899 combination of four main processes (Figure 8).

900 (1) Hydroxylation of CO_2 . Uptake of atmospheric CO_2 by “Type II” alkaline
901 spring-waters (high pH, extremely low DIC, high $[\text{Ca}^+]$, low $[\text{Mg}^{2+}]$), via rapid CO_2
902 hydroxylation reaction, results in strong depletions in $\delta^{13}\text{C}$ and $\delta^{18}\text{O}$ and enrichments in
903 Δ_{47} of carbonates. Relative to expected equilibrium values for average alkaline spring
904 conditions, the typical depletion in $\delta^{13}\text{C}$ and enrichment in Δ_{47} are approximately 1.1‰
905 and 0.011‰, respectively, for every 1‰ depletion in $\delta^{18}\text{O}$. This observed Δ_{47} - $\delta^{18}\text{O}$ slope
906 agrees quantitatively with our first-order theoretical estimation about the Δ_{47} - $\delta^{18}\text{O}$
907 correlation associated with CO_2 hydroxylation reaction.

908 (2) Partial equilibration of DIC. Although most of the atmospheric CO_2 taken up
909 by alkaline spring water is removed rapidly by the precipitation of calcium carbonate,
910 some amount of DIC may remain in the spring water. This residual DIC may gradually
911 equilibrate isotopically at ambient conditions, producing $\delta^{13}\text{C}$ - $\delta^{18}\text{O}$ - Δ_{47} trends towards
912 the expected equilibrium values and resulting in intermediate isotopic compositions
913 observed in both fresh precipitates in shallow alkaline spring outlets and layered
914 travertines.

915 (3) Mixing of different carbonate end-members. (a) When surface runoff enters
916 alkaline pools, DIC in these runoff waters, which should already be isotopically
917 equilibrated with ambient surface conditions, allows for the precipitation of calcium

918 carbonate (mostly aragonite) with equilibrium values of $\delta^{13}\text{C}$, $\delta^{18}\text{O}$, and Δ_{47} . Bottom floe
919 samples that are a mixture of this runoff-derived carbonate and carbonate formed by
920 direct reaction of atmospheric CO_2 with alkaline spring water, define mixing trends that
921 are characterized by positive mixing anomalies in Δ_{47} and slightly shallower $\delta^{13}\text{C}$ - $\delta^{18}\text{O}$
922 correlations. The shallower slope of these $\delta^{13}\text{C}$ - $\delta^{18}\text{O}$ correlations reflects greater
923 influence of soil CO_2 in surface runoff waters, whose $\delta^{13}\text{C}$ is lower than that of
924 atmospheric CO_2 . (b) Non-linear clumped isotope mixing trends are also evident in
925 subsamples of some older travertine specimen, characterizing the mixing between
926 preserved travertines and later generations of carbonate precipitated within their pore
927 spaces. Although such samples may still lie along the typical travertine $\delta^{13}\text{C}$ - $\delta^{18}\text{O}$
928 correlations, anomalous enrichments of Δ_{47} at intermediate $\delta^{13}\text{C}$ and $\delta^{18}\text{O}$ values are
929 indicative of mixing between isotopically distinct end end-members.

930 (4) Recrystallization of preserved travertines. Unlike fresh carbonate precipitates,
931 some preserved travertines record $\delta^{13}\text{C}$, $\delta^{18}\text{O}$, and Δ_{47} values close to equilibrium with
932 average conditions in alkaline springs and groundwater in Oman. We suggest that these
933 isotope compositions could have been attained by isotopic exchange during post-
934 depositional recrystallization. Other preserved travertines overlap in isotope composition
935 with recently-formed travertines and fresh carbonate precipitates, suggesting that
936 recrystallization affects some, but not all, older travertine terraces. The extent of this
937 recrystallization process may be controlled by the initial carbonate mineralogy (e.g.,
938 replacement of aragonite with calcite) and/or changes in hydrology of the travertine
939 terrace over time (e.g., some portions of travertine terraces will be subject to more post-
940 depositional interaction with water than others).

941

942 **5.4 Potential applications**

943 The overall trends in $\delta^{13}\text{C}$, $\delta^{18}\text{O}$, and Δ_{47} discussed above can be applied to
944 distinguish alkaline spring processes from other processes generating correlations in
945 carbonate $\delta^{13}\text{C}$ and $\delta^{18}\text{O}$ and to identify mixing of different carbonate end-members. Both
946 of these are often not possible when examining the bulk $\delta^{13}\text{C}$, $\delta^{18}\text{O}$ compositions of
947 carbonates alone.

948

949 *5.4.1 Identification of carbonate from subaerial hyperalkaline systems*

950 Correlation between enrichments in Δ_{47} and depletions in $\delta^{13}\text{C}$ and $\delta^{18}\text{O}$ could
951 serve as a marker to identify carbonates formed by rapid uptake of CO_2 in subaerial
952 alkaline environments. $\delta^{13}\text{C}$ and $\delta^{18}\text{O}$ data alone are insufficient for identifying these
953 processes, as $\delta^{13}\text{C}$ - $\delta^{18}\text{O}$ trends similar in slope and range to those observed in alkaline
954 spring systems can be produced by other processes as well. For example, correlated $\delta^{13}\text{C}$
955 and $\delta^{18}\text{O}$ variations are also observed in carbonate cements in conglomerates from Sur,
956 Oman, but are thought to reflect variations in the isotopic composition of surface waters
957 due to past changes in rainfall patterns and vegetation (Burns and Matter, 1995). Because
958 the $\delta^{13}\text{C}$ - $\delta^{18}\text{O}$ trends in those carbonates are not related to the kinetic processes described
959 here, they would be expected to record equilibrium Δ_{47} values. Similarly, it might be
960 unclear in some cases whether depletions in carbonate $\delta^{13}\text{C}$ and $\delta^{18}\text{O}$ are due to kinetic
961 effects associated with uptake of CO_2 in alkaline environments or inherited from
962 dissolution of carbonate bedrock, e.g., calcium carbonates precipitated during weathering
963 of ultramafic mine tailings (Wilson et al., 2009). Clumped isotope analysis could be a

964 useful diagnostic in these cases. If depletions in $\delta^{13}\text{C}$ and $\delta^{18}\text{O}$ correlate with enrichments
965 in Δ_{47} , kinetic effects during hydroxylation of CO_2 would be indicated.

966 This same correlation between $\delta^{18}\text{O}$ and Δ_{47} could also be applied to identify
967 extinct alkaline spring systems in terrestrial and extraterrestrial environments. For
968 example, the slope and magnitude of $\delta^{13}\text{C}$ - $\delta^{18}\text{O}$ variations in carbonates in Martian
969 meteorites are similar to that observed in carbonates from terrestrial alkaline springs, and
970 serpentinization-related hyperalkaline systems have been suggested as possible sources of
971 methane generation and carbonate precipitation on Mars (e.g., Niles et al., 2005; Oze and
972 Sharma, 2005; Ehlmann et al., 2010; Etiope et al., 2013). Identification of a Δ_{47} trend in
973 Martian carbonates similar to trends observed in fresh precipitates and associated
974 travertines in Oman could suggest that hyperalkaline springs were present on the surface
975 of Mars, and may provide further constraints on surface environments on Mars. In one
976 clumped isotope study of Martian carbonates, no such correlation was observed (Halevy
977 et al., 2011). However, as a result of the precious nature of these Martian samples and the
978 challenges to perform the clumped analysis on such small amounts of samples, only a
979 relatively small range of $\delta^{13}\text{C}$ and $\delta^{18}\text{O}$ variations were observed in the limited number of
980 analyses in that study (7.8‰ and 5.9‰ respectively), which could obscure variations in
981 Δ_{47} expected from the kinetic trends.

982

983 *5.4.2 Mixing trends: Identification of carbonate mixing and paleoclimate reconstruction*

984 Due to the non-linear nature of mixing in Δ_{47} , clumped isotope anomalies can be
985 one of the clearest indicators of mixing between carbonates with distinct bulk stable
986 isotopic compositions.

987 In fresh bottom flocc samples from larger alkaline pools, we are able to identify a
988 mixing end-member corresponding to equilibrium with temperatures consistent with
989 winter rainfall in Oman. The laminated travertines analyzed in this study are not likely to
990 have formed under similar conditions as these bottom flocc samples, and thus do not
991 reflect the same kind of mixing process. However, it is possible that other travertines in
992 Oman have formed in a pool-bottom environment and would preserve the mixing
993 signatures with an equilibrium end-member recording rainy season conditions. In its
994 current arid climate, Oman receives most of its rainfall in the winter months, but it has
995 experienced wetter climates in the past where rainfall was dominated by the summer
996 monsoon (Clark and Fontes, 1990; Burns et al., 2001; Fleitmann et al., 2003). Carbonate
997 formed in pool bottoms of alkaline springs during those periods could record a mixing
998 end-member in equilibrium with summertime temperatures, allowing identification of
999 major shifts in precipitation patterns that are not available from their bulk stable isotope
1000 compositions.

1001 Δ_{47} mixing trends observed in the subsamples of our older travertine samples,
1002 reflecting influence of later generations of carbonate precipitation, suggest caution needs
1003 to be taken when interpreting ^{14}C age and paleoclimate data from travertines formed at
1004 alkaline spring outlets (Appendix B). The non-linear nature of Δ_{47} mixing makes it a
1005 valuable tool to identify suites of samples that have been affected by later generations of
1006 carbonate precipitation, which is not readily apparent from the $\delta^{13}\text{C}$ - $\delta^{18}\text{O}$ trends alone.
1007 Conversely, travertines whose Δ_{47} reflect the same processes observed in fresh
1008 precipitates at alkaline springs are likely to provide robust ^{14}C ages and information about
1009 their formation conditions.

1010

1011 **6. Conclusions**

1012 Carbonates precipitated during atmospheric CO₂ uptake by hyperalkaline springs
1013 in Oman record significant enrichments in Δ_{47} correlated with depletions in $\delta^{13}\text{C}$ and
1014 $\delta^{18}\text{O}$. These kinetic isotope effects are the result of hydroxylation of CO₂ under high pH
1015 conditions and are best reflected in fresh calcite films formed at the air-water interface.
1016 Partial equilibration of the DIC in alkaline springs may shift the clumped isotope and
1017 bulk stable isotopic compositions of some bottom floc samples away from this most
1018 fractionated end-member along a trend toward expected equilibrium values. These
1019 processes are reflected in both fresh precipitates from alkaline springs and associated
1020 preserved travertines, though some older travertines may have experienced isotopic re-
1021 equilibration.

1022 Because mixing is nonlinear in Δ_{47} , mixing of two isotopically distinct carbonates
1023 can be distinguished from equilibration trends or other processes that can also cause
1024 correlated variations in $\delta^{13}\text{C}$ and $\delta^{18}\text{O}$. In fresh bottom floc samples from hyperalkaline
1025 springs in Oman, this allows us to identify mixing between the above disequilibrium end-
1026 member and possible equilibrium end-members. The nonlinear nature of the clumped
1027 isotope signature during mixing also makes it possible to identify travertine samples that
1028 may have been affected by later generations of carbonate precipitation within the
1029 travertine pore spaces. The presence of such subsequent carbonate precipitates
1030 complicates the interpretation of the ¹⁴C age and paleoclimate data from travertines.
1031 Mixed analyses may not be easily identified from $\delta^{18}\text{O}$, $\delta^{13}\text{C}$, and ¹⁴C trends, whereas

1032 Δ_{47} - $\delta^{18}\text{O}$ - $\delta^{13}\text{C}$ trends may show distinctive positive Δ_{47} anomalies at intermediate $\delta^{18}\text{O}$
1033 and $\delta^{13}\text{C}$ values for samples affected by mixing.

1034 Clumped isotope analysis thus provides a range of details about complex
1035 processes occurring during the precipitation and preservation of carbonates at
1036 hyperalkaline springs which are not readily apparent from $\delta^{18}\text{O}$, $\delta^{13}\text{C}$, and ^{14}C data alone.
1037

1038 **Acknowledgments**

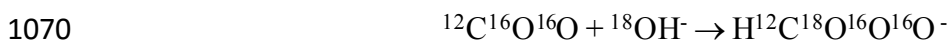
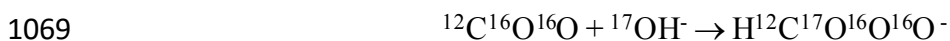
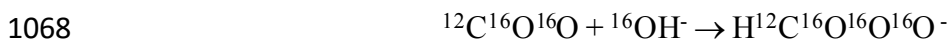
1039 Special thanks to everyone at the Ministry of Regional Municipalities and Water
1040 Resources, Sultanate of Oman, particularly Dr. Abdulaziz Ali-Al-Mashikhi and Salim Al
1041 Khanbashi, everyone at the Geological Survey of Oman and the Directorate General of
1042 Minerals in the Ministry of Commerce and Industry, particularly Dr. Ali Al Rajhi and
1043 Mohammed Al Batashi. Everett Shock, Peter Canovas, Jeff Havig, Jackie Gauntlett, and
1044 other members of the Oman field teams are thanked for their assistance with fieldwork
1045 and scientific discussions. We thank Dr. Frieder Klein for providing the access to the
1046 Raman spectrometer and Dr. Susan Humphris for help in the sample selection. This work
1047 was supported by the Howland Postdoctoral Scholarship at WHOI to E. Falk; NSF-ANT-
1048 1246387 and the Investment in Science Fund at WHOI to W. Guo; NSF Graduate
1049 Research Fellowships to A. Paukert and E. Falk; funding from Petroleum Development
1050 Oman, Lamont-Doherty Earth Observatory, and a Columbia Research Initiative in
1051 Science and Engineering grant to P. Kelemen and J. Matter; the Arthur D. Storke Chair at
1052 Columbia University, NSF-MGG-1059175, and NSF-EAR-1049905 to P. Kelemen.
1053

1054 **Appendix A. Estimation of the oxygen isotope and clumped isotope composition of**
1055 **HCO₃⁻ derived from CO₂ hydroxylation reaction**

1056 The CO₂ hydroxylation reaction is ubiquitous in aqueous solutions containing
1057 dissolved inorganic carbon:



1059 In high pH solutions, CO₂ hydroxylation is the dominant reaction path by which CO₂
1060 converts to HCO₃⁻ (McConnaughey, 1989). To obtain a first order estimation on the
1061 oxygen isotope and clumped isotope composition of the HCO₃⁻ derived from CO₂
1062 hydroxylation, we assume (1) there is no kinetic isotope fractionation associated with
1063 CO₂ hydroxylation, i.e. the addition of OH⁻ is random, and (2) the isotopic compositions
1064 of both CO₂ and OH⁻ are in equilibrium with water at assumed temperatures (Clark et al.,
1065 1992; Rollion-Bard et al., 2003). We then calculate the abundances of different HCO₃⁻
1066 isotopologues, by considering the reactions between all 12 stable isotopologues of CO₂
1067 and 3 oxygen isotopologues of OH⁻:



1071



1075

1076 The abundances of different CO₂ isotopologues at assumed temperatures are calculated
1077 following the methodology and algorithms described by Wang et al. (2004).
1078 At 300K, for $\delta^{13}\text{C}_{\text{CO}_2, \text{VPDB}} = 0\text{‰}$ and $\delta^{18}\text{O}_{\text{water, VSMOW}} = 0\text{‰}$, our calculation yields
1079 $\delta^{18}\text{O}_{\text{CO}_2, \text{VSMOW}} = 41.6\text{‰}$, $\delta^{18}\text{O}_{\text{OH}^-, \text{VSMOW}} = -37.6\text{‰}$ and $\Delta_{47, \text{CO}_2} = 0.924\text{‰}$
1080 (Brenninkmeijer et al., 1983; Green and Taube, 1963; Wang et al., 2004). Accordingly,
1081 the isotopic composition of the HCO₃⁻ derived from CO₂ hydroxylation reaction is
1082 estimated to be $\delta^{13}\text{C}_{\text{HCO}_3^-, \text{VPDB}} = 0\text{‰}$, $\delta^{18}\text{O}_{\text{HCO}_3^-, \text{VSMOW}} = 15.2\text{‰}$, and $\Delta_{63} = 0.590\text{‰}$,
1083 where Δ_{63} denotes the extent of ¹³C-¹⁸O clumping (mostly) in the HCO₃⁻ and is defined
1084 the same way as in Guo et al. (2009). This estimated isotope composition of HCO₃⁻ is
1085 depleted in ¹⁸O but enriched in Δ_{63} , compared to the expected equilibrium isotope
1086 composition of HCO₃⁻ at 300K (i.e., $\delta^{18}\text{O}_{\text{HCO}_3^-, \text{VSMOW}} = 30.7\text{‰}$, $\Delta_{63} = 0.397\text{‰}$; Beck et
1087 al., 2005; Hill et al., 2014), with an apparent Δ_{63} -¹⁸O slope of -0.012. In high pH
1088 solutions, CO₃²⁻ comprises a far greater proportion of the DIC pool than HCO₃⁻, but
1089 isotopic equilibration between HCO₃⁻ and CO₃²⁻ is effectively instantaneous, with an
1090 equilibrium Δ_{63} fractionation of 0.033-0.063‰ (McConnaughey, 1989; Tripathi et al.,
1091 2015). Therefore, the magnitude of clumped isotope enrichment and ¹⁸O depletion in the
1092 total DIC pool will be inherited from the HCO₃⁻ formed during the hydroxylation
1093 reaction. This is expected to lead to an apparent Δ_{47} -¹⁸O slope of the same magnitude in
1094 the carbonate solids derived from CO₂ hydroxylation reaction (Section 5.1.1, Guo et al.,
1095 2009).

1096

1097 **Appendix B. Effects of carbonate mixing on apparent ^{14}C ages of travertine**

1098 Precipitation of later generations of carbonates within the pore space of the travertine
1099 (e.g. in preserved travertine terrace OM10-32C), if unaccounted for, can result in
1100 significant errors in estimating the true formation ages of travertine samples based on ^{14}C
1101 method (Section 5.2.2). To illustrate this, we calculate possible ranges of “true” ages for
1102 the initial formation of travertine OM10-32C subsamples.

1103 We assume that the precipitation of “contaminant” carbonate within the travertine
1104 pore space occurred at the same time for all sub-samples and did not incorporate any
1105 dead carbon. Under these assumptions, the fraction modern carbon (F_m) of the
1106 hypothetical contaminant end-member is constrained by the maximum measured F_m in
1107 the travertine subsamples and the minimum possible “true” F_m . In other words, the
1108 hypothetical contaminant end-member cannot be older than the most recent travertine
1109 subsample, and it cannot be so young that the calculated “true” F_m would be less than
1110 zero for any subsample. We then calculate the “true” F_m and corresponding ^{14}C age of
1111 each subsample that would produce their measured apparent ages, using the proportions
1112 of hypothetical contaminant carbonates estimated in Section 5.2.2 and shown in Figure 7.

1113 Depending on the assumed value for the F_m of the contaminant end-member, the
1114 calculated “true” ages of the travertine can be tens of thousands of years older than their
1115 apparent ^{14}C ages and even relative order of formation for the subsamples can change
1116 (Table B.1, Figure B.1). Note, in reality, the contaminant carbonates could have formed
1117 over multiple episodes or could have incorporated dead carbon. Therefore, the true ages
1118 of the travertine can be even less well-constrained.

1119

1120 **References**

- 1121 Affek H. P. (2012) Clumped isotope paleothermometry: Principles, applications, and
1122 challenges. In *Reconstructing Earth's Deep-Time Climate – The State of the Art*
1123 *in 2012*. (eds. Ivany, L. C., Huber, B.). Paleontological Society Papers, pp. 101-
1124 114.
- 1125 Affek H. P. and Eiler J. M. (2006) Abundance of mass 47 CO₂ in urban air, car exhaust,
1126 and human breath. *Geochim. Cosmochim. Acta* **70**, 1-12.
- 1127 Affek H. P., Bar-Matthews M., Ayalon A., Matthews A. and Eiler J. M. (2008)
1128 Glacial/interglacial temperature variations in Soreq cave speleothems as recorded
1129 by 'clumped isotope' thermometry. *Geochim. Cosmochim. Acta* **72**, 5351-5360.
- 1130 Affek H. P., Matthews A., Ayalon A., Bar-Matthews M., Burstyn Y., Zaarur S. and
1131 Zilberman T. (2014) Accounting for kinetic isotope effects in Soreq Cave (Israel)
1132 speleothems. *Geochim. Cosmochim. Acta* **143**, 303-318.
- 1133 Barnes I. and O'Neil J. R. (1969) Relationship between fluids in some fresh alpine-type
1134 ultramafics and possible modern serpentinization, western United States. *GSA*
1135 *Bull.* **80**, 1947-1960.
- 1136 Barnes I., LaMarche V. C. and Himmelberg G. (1967) Geochemical evidence of present-
1137 day serpentinization. *Science* **156**, 830-832.
- 1138 Barnes I., O'Neil J. R. and Trescases J. J. (1978) Present Day Serpentinization in New-
1139 Caledonia, Oman and Yugoslavia. *Geochim. Cosmochim. Acta* **42**, 144-145.
- 1140 Beck W. C., Grossman E. L. and Morse J. W. (2005) Experimental studies of oxygen
1141 isotope fractionation in the carbonic acid system at 15°, 25°, and 40°C. *Geochim.*
1142 *Cosmochim. Acta* **69**, 3493-3503.
- 1143 Boudier F. and Coleman R. G. (1981) Cross section through the peridotite in the Semail
1144 ophiolite. *J. Geophys. Res.* **86**, 2573-2592.
- 1145 Boudier F., Baronnet A. and Mainprice D. (2010) Serpentine mineral replacements of
1146 natural olivine and their seismic implications: Oceanic lizardite versus
1147 subduction-related antigorite. *J. Petrol.* **51**, 495-512.
- 1148 Brenninkmeijer, C.A.M., Kraft, P. and Mook, W.G. (1983) Oxygen isotope fractionation
1149 between CO₂ and H₂O. *Isot. Geosci.* **1**, 181-190.
- 1150 Bruni J., Canepa M., Chiodini G., Cioni R., Cipolli F., Longinelli A., Marini L., Ottonello
1151 G. and Zuccolini M. V. (2002) Irreversible water-rock mass transfer
1152 accompanying the generation of the neutral, Mg-HCO₃ and high-pH, Ca-OH
1153 spring waters of the Genova province, Italy. *Appl. Geochem.* **17**, 455-474.

- 1154 Burns S. J. and Matter A. (1995) Geochemistry of Carbonate Cements in Surficial
1155 Alluvial Conglomerates and Their Paleoclimatic Implications, Sultanate-of-
1156 Oman. *J. Sediment. Res. A* **65**, 170-177.
- 1157 Burns S. J., Fleitmann D., Matter A., Neff U. and Mangini A. (2001) Speleothem
1158 evidence from Oman for continental pluvial events during interglacial periods.
1159 *Geology* **29**, 623-626.
- 1160 Cardace D., Meyer-Dombard D. A. R., Woycheese K. and Arcilla C. A. (2015) Feasible
1161 Metabolic Schema Associated with High pH Springs in the Philippines. *Front.*
1162 *Microbiol.* **6**.
- 1163 Chavagnac V., Ceuleneer G., Monnin C., Lansac B., Hoareau G. and Boulart C. (2013a)
1164 Mineralogical assemblages forming at hyperalkaline warm springs hosted on
1165 ultramafic rocks: A case study of Oman and Ligurian ophiolites. *Geochem.*
1166 *Geophys. Geosys.* **14**, 2474-2495
- 1167 Chavagnac V., Monnin C., Ceuleneer G., Boulart C. and Hoareau G. (2013b)
1168 Characterization of hyperalkaline fluids produced by low-temperature
1169 serpentinization of mantle peridotites in the Oman and Ligurian ophiolites.
1170 *Geochem. Geophys. Geosys.* **14**, 2496-2522.
- 1171 Cipolli F., Gambardella B., Marini L., Ottonello G. and Zuccolini M. V. (2004)
1172 Geochemistry of high-pH waters from serpentinites of the Gruppo di Voltri
1173 (Genova, Italy) and reaction path modeling of CO₂ sequestration in serpentinite
1174 aquifers. *Appl. Geochem.* **19**, 787-802.
- 1175 Clark I. D. and Fontes J. C. (1990) Paleoclimatic reconstruction in northern Oman based
1176 on carbonates from hyperalkaline groundwaters. *Quaternary Res.* **33**, 320-336.
- 1177 Clark I. D., Fontes J. C. and Fritz P. (1992) Stable isotope disequilibria in travertine from
1178 high pH-waters - Laboratory investigations and field observations from Oman.
1179 *Geochim. Cosmochim. Acta* **56**, 2041-2050.
- 1180 Craig H. (1961) Isotopic variations in meteoric waters. *Science* **133**, 1702-1703.
- 1181 Daeron M., Guo W., Eiler J., Genty D., Blamart D., Boch R., Drysdale R., Maire R.,
1182 Wainer K. and Zanchetta G. (2011) (CO)-C-13-O-18 clumping in speleothems:
1183 Observations from natural caves and precipitation experiments. *Geochim.*
1184 *Cosmochim. Acta* **75**, 3303-3317.
- 1185 Defliese W. F., Hren M. T. and Lohmann K.C. (2015) Compositional and temperature
1186 effects of phosphoric acid fractionation on $\Delta 47$ analysis and implications for
1187 discrepant calibrations. *Chem. Geol.*, **396**, 51-60.
- 1188 Defliese W. F. and Lohmann K. C. (2015) Non-linear mixing effects on mass-47 CO₂
1189 clumped isotope thermometry: Patterns and implications. *Rapid Commun. Mass*
1190 *Sp.* **29**, 901-909.

- 1191 Dennis K. J. and Schrag D. P. (2010) Clumped isotope thermometry of carbonatites as an
1192 indicator of diagenetic alteration. *Geochim. Cosmochim. Acta* **74**, 4110-4122.
- 1193 Dennis K. J., Affek H. P., Passey B. H., Schrag D. P. and Eiler J. M. (2011) Defining an
1194 absolute reference frame for 'clumped' isotope studies of CO₂. *Geochim.*
1195 *Cosmochim. Acta* **75**, 7117-7131.
- 1196 Dietzel M., Usdowski E. and Hoefs J. (1992) Chemical and C-13/C-12-isotope and O-
1197 18/O-16-isotope evolution of alkaline drainage waters and the precipitation of
1198 calcite. *Appl. Geochem.* **7**, 177-184.
- 1199 Eagle R. A., Eiler J. M., Tripathi A. K., Ries J. B., Freitas P. S., Hiebenthal C.,
1200 Wanamaker A. D., Taviani M., Elliot M., Marensi S., Nakamura K., Ramirez P.
1201 and Roy K. (2013) The influence of temperature and seawater carbonate
1202 saturation state on ¹³C-¹⁸O bond ordering in bivalve mollusks. *Biogeosciences* **10**,
1203 4591-4606. Ehlmann B. L., Mustard J. F. and Murchie S. L. (2010) Geologic
1204 setting of serpentine deposits on Mars. *Geophys. Res. Lett.* **37**.
- 1205 Eiler J. (2007) "Clumped-isotope" geochemistry: The study of naturally occurring,
1206 multiply-substituted isotopologues. *Earth Planet. Sci. Lett.* **262**, 309-327.
- 1207 Eiler J. M. (2011) Paleoclimate reconstruction using carbonate clumped isotope
1208 thermometry. *Quaternary Sci. Rev.* **30**, 3575-3588.
- 1209 Eiler J. M. and Schauble E. (2004) (OCO)-O-18-C-13-O-16 in Earth's atmosphere.
1210 *Geochim. Cosmochim. Acta* **68**, 4767-4777.
- 1211 Epstein S. and Mayeda T. (1953) Variation of O18 content of waters from natural
1212 sources. *Geochim. Cosmochim. Acta* **4**, 213-224.
- 1213 Etiope G., Ehlmann B. L. and Schoell M. (2013) Low temperature production and
1214 exhalation of methane from serpentinized rocks on Earth: A potential analog for
1215 methane production on Mars. *Icarus* **224**, 276-285.
- 1216 Falk E. S. (2013) Carbonation of peridotite in the Oman ophiolite. Ph.D. thesis, Columbia
1217 University.
- 1218 Falk E. S. and Kelemen P. B. (2015) Geochemistry and petrology of listvenite in the
1219 Samail ophiolite, Sultanate of Oman: Complete carbonation of peridotite during
1220 ophiolite emplacement. *Geochim. Cosmochim. Acta* **160**, 70-90.
- 1221 Fleitmann D., Burns S. J., Neff U., Mangini A. and Matter A. (2003) Changing moisture
1222 sources over the last 330,000 years in Northern Oman from fluid-inclusion
1223 evidence in speleothems. *Quaternary Res.* **60**, 223-232.
- 1224 Gehre M., Hoefling R., Kowski P. and Strauch G. (1996) Sample preparation device for
1225 quantitative hydrogen iso-tope analysis using chromium metal. *Anal. Chem.* **68**,
1226 4414-4417.

- 1227 Ghosh P., Adkins J., Affek H., Balta B., Guo W., Schauble E. A., Schrag D. and Eiler J.
1228 M. (2006) 13C–18O bonds in carbonate minerals: A new kind of
1229 paleothermometer. *Geochim. Cosmochim. Acta* **70**, 1439-1456.
- 1230 Godard M., Jousset D. and Bodinier J.-L. (2000) Relationships between geochemistry
1231 and structure beneath a palaeo-spreading centre: a study of the mantle section in
1232 the Oman ophiolite. *Earth Planet. Sci. Lett.* **180**, 133-148.
- 1233 Guo W. (2008) Carbonate clumped isotope thermometry : application to carbonaceous
1234 chondrites and effects of kinetic isotope fractionation. Ph.D. thesis, California
1235 Institute of Technology.
- 1236 Guo W. F., Mosenfelder J. L., Goddard W. A. and Eiler J. M. (2009) Isotopic
1237 fractionations associated with phosphoric acid digestion of carbonate minerals:
1238 Insights from first-principles theoretical modeling and clumped isotope
1239 measurements. *Geochim. Cosmochim. Acta* **73**, 7203-7225.
- 1240 Grauel A.-L., Schmid T. W., Hu B., Bergami C., Capotondi L., Zhou L., Bernasconi S.
1241 M. (2013) Calibration and application of the ‘clumped isotope’ thermometer to
1242 foraminifera for high-resolution climate reconstructions. *Geochim. Cosmochim.*
1243 *Acta* **108**, 125–140
- 1244 Green M. and Taube H. (1963) Isotopic fractionation in the OH⁻-H₂O exchange reaction.
1245 *J. Phys. Chem.* **67**, 1565- 1566.
- 1246 Halevy I., Fischer W. W. and Eiler J. M. (2011) Carbonates in the Martian meteorite
1247 Allan Hills 84001 formed at 18 +/- 4 degrees C in a near-surface aqueous
1248 environment. *Proc. Natl. Acad. Sci. U.S.A.* **108**, 16895-16899.
- 1249 Hanghøj K., Kelemen P. B., Hassler D. and Godard M. (2010) Composition and genesis
1250 of depleted mantle peridotites from the Wadi Tayin massif, Oman ophiolite:
1251 Major and trace element geochemistry, and Os isotope and PGE systematics. *J.*
1252 *Petrol.* **51**, 206-227.
- 1253 Henkes G. A., Passey B. H., Wanamaker, Jr., A. D., Grossman E. L., Ambrose, Jr., W. G.
1254 and Carroll M. L. (2013) Carbonate clumped isotope compositions of modern
1255 marine mollusk and brachiopod shells. *Geochim. Cosmochim. Acta* **106**, 307-325.
- 1256 Hill P. S., Tripathi A. K. and Schauble E. A. (2014) Theoretical constraints on the effects
1257 of pH, salinity, and temperature on clumped isotope signatures of dissolved
1258 inorganic carbon species and precipitating carbonate minerals. *Geochim.*
1259 *Cosmochim. Acta* **125**, 610-652.
- 1260 Huntington K. W. and Lechler A. R. (2015) Carbonate clumped isotope thermometry in
1261 continental tectonics. *Tectonophysics* **647–648**, 1-20.
- 1262 Huntington K. W., Eiler J. M., Affek H. P., Guo W., Bonifacie M., Yeung L. Y.,
1263 Thiagarajan N., Passey B., Tripathi A., Daëron M. and Came R. (2009) Methods

- 1264 and limitations of 'clumped' CO₂ isotope ($\Delta 47$) analysis by gas-source isotope
1265 ratio mass spectrometry. *J. Mass Spectrom.* **44**, 1318-1329.
- 1266 Kele S., Breitenbach S. F., Capezzuoli E., Meckler A. N., Ziegler M., Millan I. M., Kluge
1267 T., Deák J., Hanselmann K., John C. M. and Yan H. (2015) Temperature
1268 dependence of oxygen- and clumped isotope fractionation in carbonates: A study
1269 of travertines and tufas in the 6–95 C temperature range. *Geochim. Cosmochim.*
1270 *Acta* **168**, 172-192.
- 1271 Kelemen P. B. and Matter J. (2008) In situ carbonation of peridotite for CO₂ storage.
1272 *Proc. Natl. Acad. Sci. U. S. A.* **105**, 17295-17300.
- 1273 Kelemen P. B., Matter J., Streit E. E., Rudge J. F., Curry W. B. and Bluztajn J. (2011)
1274 Rates and mechanisms of mineral carbonation in peridotite: Natural processes and
1275 recipes for enhanced, in situ CO₂ capture and storage. *Ann. Rev. Earth Planet. Sci.*
1276 **39**, 545-576.
- 1277 Kim S. T. and O'Neil J. R. (1997) Equilibrium and nonequilibrium oxygen isotope effects
1278 in synthetic carbonates. *Geochim. Cosmochim. Acta* **61**, 3461-3475.
- 1279 Kim S. T., O'Neil J. R., Hillaire-Marcel C. and Mucci A. (2007) Oxygen isotope
1280 fractionation between synthetic aragonite and water: influence of temperature and
1281 Mg²⁺ concentration. *Geochim. Cosmochim. Acta* **71**, 4704-4715.
- 1282 Kluge T. and Affek H. P. (2012) Quantifying kinetic fractionation in Bunker Cave
1283 speleothems using $\Delta 47$. *Quaternary Sci. Rev.* **49**, 82-94.
- 1284 Kluge T., Affek H. P., Zhang Y. G., Dublyansky Y., Spötl C., Immenhauser A. and
1285 Richter D. K. (2014) Clumped isotope thermometry of cryogenic cave carbonates.
1286 *Geochim. Cosmochim. Acta* **126**, 541-554.
- 1287 Kluge T., John C. M., Jourdan A.-L., Davis S. and Crawshaw J. (2015) Laboratory
1288 calibration of the calcium carbonate clumped isotope thermometer in the 25–
1289 250;°C temperature range. *Geochim. Cosmochim. Acta* **157**, 213-227.
- 1290 Kosednar-Legenstein B., Dietzel M., Leis A. and Stingl K. (2008) Stable carbon and
1291 oxygen isotope investigation in historical lime mortar and plaster - Results from
1292 field and experimental study. *Appl. Geochem.* **23**, 2425-2437.
- 1293 Marques J. M., Carreira P. M., Carvalho M. R., Matias M. J., Goff F. E., Basto M. J.,
1294 Graça R. C., Aires-Barros L. and Rocha L. (2008) Origins of high pH mineral
1295 waters from ultramafic rocks, Central Portugal. *Appl. Geochem.* **23**, 3278-3289.
- 1296 Matter J. M. (2005) Recharge areas and geochemical evolution of groundwater in an
1297 alluvial aquifer system in the Sultanate of Oman. *Hydrogeology J.* **14**, 203-224.
- 1298 Matter J. M. and Kelemen P. B. (2009) Permanent CO₂ storage and mineral carbonation
1299 in geologic reservoirs. *Nat. Geosci.* **2**, 837-841.

- 1300 McConnaughey, T. (1989). ^{13}C and ^{18}O isotopic disequilibrium in biological carbonates:
1301 II. In vitro simulation of kinetic isotope effects. *Geochim. Cosmochim. Acta* **53**,
1302 163-171.
- 1303 McCrea J. M. (1950) On the Isotopic Chemistry of Carbonates and a Paleotemperature
1304 Scale. *J. Chem. Phys.* **18**, 849-857.
- 1305 Mervine E. M., Humphris S. E., Sims K. W. W., Kelemen P. B. and Jenkins W. J. (2014)
1306 Carbonation rates of peridotite in the Samail Ophiolite, Sultanate of Oman,
1307 constrained through ^{14}C dating and stable isotopes. *Geochim. Cosmochim. Acta*
1308 **126**, 371-397.
- 1309 Mervine E. M., Sims K. W. W., Humphris S. E. and Kelemen P. B. (2015) Applications
1310 and limitations of U–Th disequilibria systematics for determining ages of
1311 carbonate alteration minerals in peridotite. *Chem. Geol.* **412**, 151-166.
- 1312 Monnier C., Girardeau J., Le Mée L. and Polvé M. (2006) Along-ridge petrological
1313 segmentation of the mantle in the Oman ophiolite. *Geochem. Geophys. Geosys.* **7**.
- 1314 Neal C. and Stanger G. (1983) Hydrogen generation from mantle source rocks in Oman.
1315 *Earth Planet. Sci. Lett.* **66**, 315-320.
- 1316 Neal C. and Stanger G. (1985) Past and present serpentinization of ultramafic rocks: An
1317 example from the Semail ophiolite nappe of northern Oman, in: Drewer, J. I.
1318 (Ed.), *The Chemistry of Weathering*. D. Reidel Publishing Company, Holland, pp.
1319 249-275.
- 1320 Neal C. and Shand P. (2002) Spring and surface water quality of the Cyprus ophiolites.
1321 *Hydrol. Earth Sys. Sci.* **6**, 797-817.
- 1322 Niles P. B., Leshin L. A. and Guan Y. (2005) Microscale carbon isotope variability in
1323 ALH84001 carbonates and a discussion of possible formation environments.
1324 *Geochim. Cosmochim. Acta* **69**, 2931-2944.
- 1325 Niles P., Catling D., Berger G., Chassefière E., Ehlmann B., Michalski J., Morris R., Ruff
1326 S. and Sutter B. (2013) Geochemistry of Carbonates on Mars: Implications for
1327 Climate History and Nature of Aqueous Environments. *Space Sci. Rev.* **174**, 301-
1328 328.
- 1329 Olsson I. U. (1970) The use of oxalic acid as a standard. In *Radiocarbon Variations and*
1330 *Absolute Chronology, Nobel Symposium, 12th Proc.*, John Wiley and Sons, New
1331 York, p. 17.
- 1332 Oman Directorate General of Meteorology (2015) Nizwa historical climate data, 1986-
1333 2009. [http://www.met.gov.om/opencms/export/sites/default/dgman/en/weather-](http://www.met.gov.om/opencms/export/sites/default/dgman/en/weather-chart/historical-data/)
1334 [chart/historical-data/](http://www.met.gov.om/opencms/export/sites/default/dgman/en/weather-chart/historical-data/)

- 1335 O'Neil J. R. and Barnes I. (1971) C13 and O18 compositions in some fresh-water
1336 carbonates associated with ultramafic rocks and serpentinites: western United
1337 States. *Geochim. Cosmochim. Acta* **35**, 687-697.
- 1338 Oze C. and Sharma M. (2005) Have olivine, will gas: Serpentinization and the abiogenic
1339 production of methane on Mars. *Geophys. Res. Lett.* **32**, L10203.
- 1340 Paukert A. N., Matter J. M., Kelemen P. B., Shock E. L. and Havig J. R. (2012) Reaction
1341 path modeling of enhanced in situ CO₂ mineralization for carbon sequestration in
1342 the peridotite of the Samail Ophiolite, Sultanate of Oman. *Chem. Geol.* **330-331**,
1343 86-100.
- 1344 Reimer P., Bard E., Bayliss A., Beck J., Blackwell P., Bronk Ramsey C., Buck C., Cheng
1345 H., Edwards R., Friedrich M., Grootes P., Guilderson T., Hafliðason H., Hajdas I.,
1346 Hatté C., Heaton T., Hoffmann D., Hogg A., Hughen K., Kaiser K., Kromer B.,
1347 Manning S., Niu M., Reimer R., Richards D., Scott E., Southon J., Staff R.,
1348 Turney C. and van der Plicht J. (2013) IntCal13 and Marine13 radiocarbon age
1349 calibration curves 0–50,000 years cal BP. *Radiocarbon*, **55**(4), 1869-1887.
- 1350 Rollion-Bard C., Chaussidon M. and France-Lanord C. (2003) pH control on oxygen
1351 isotopic composition of symbiotic corals. *Earth Planet. Sci. Lett.* **215**, 275-288.
- 1352 Saenger C., Affek H. P., Felis T., Thiagarajan N., Lough J. M. and Holcomb M. (2012)
1353 Carbonate clumped isotope variability in shallow water corals: Temperature
1354 dependence and growth-related vital effects. *Geochim. Cosmochim. Acta* **99**, 224-
1355 242.
- 1356 Schmid T. W. (2011) Clumped isotopes: a new tool for old questions. Ph.D. thesis,
1357 Eidgenössische Technische Hochschule ETH Zürich.
- 1358 Spooner P. T., Guo W., Robinson L. F., Thiagarajan N., Hendry K., Rosenheim B. E. and
1359 Leng M. J. (2016) Clumped isotope composition of cold-water corals: A role for
1360 vital effects? *Geochim. Cosmochim. Acta.* **179**, 123-141.
- 1361 Streit E., Kelemen P. and Eiler J. (2012) Coexisting serpentine and quartz from
1362 carbonate-bearing serpentinized peridotite in the Samail Ophiolite, Oman.
1363 *Contrib. Mineral. Petr.* **164**, 821-837.
- 1364 Szponar N., Brazelton W. J., Schrenk M. O., Bower D. M., Steele A. and Morrill P. L.
1365 (2013) Geochemistry of a continental site of serpentinization, the Tablelands
1366 Ophiolite, Gros Morne National Park: A Mars analogue. *Icarus* **224**, 286-296.
- 1367 Tang J., Dietzel M., Fernandez A., Tripathi A. K. and Rosenheim B. E. (2014) Evaluation
1368 of kinetic effects on clumped isotope fractionation ($\Delta 47$) during inorganic calcite
1369 precipitation. *Geochim. Cosmochim. Acta* **134**, 120-136.

- 1370 Thiagarajan N., Adkins J. and Eiler J. (2011) Carbonate clumped isotope thermometry of
1371 deep-sea corals and implications for vital effects. *Geochim. Cosmochim. Acta* **75**,
1372 4416-4425.
- 1373 Thornalley D. J. R., Bauch H. A., Gebbie G., Guo W., Ziegler M., Bernasconi S. M.,
1374 Barker S., Skinner L. C. and Yu J. (2015) A warm and poorly ventilated deep
1375 Arctic Mediterranean during the last glacial period. *Science* **349**, 706-710.
- 1376 Tripathi A. K., Eagle R. A., Thiagarajan N., Gagnon A. C., Bauch H., Halloran P. R. and
1377 Eiler J. M. (2010) C-13-O-18 isotope signatures and 'clumped isotope'
1378 thermometry in foraminifera and coccoliths. *Geochim. Cosmochim. Acta* **74**,
1379 5697-5717.
- 1380 Tripathi A. K., Hill P. S., Eagle R. A., Mosenfelder J. L., Tang J., Schauble E. A., Eiler J.
1381 M., Zeebe R. E., Uchikawa J., Coplen T. B., Ries J. B. and Henry D. (2015)
1382 Beyond temperature: Clumped isotope signatures in dissolved inorganic carbon
1383 species and the influence of solution chemistry on carbonate mineral composition.
1384 *Geochim. Cosmochim. Acta* **166**, 344-371.
- 1385 Wainer K., Genty D., Blamart D., Daëron M., Bar-Matthews M., Vonhof H., Dublyansky
1386 Y., Pons-Branchu E., Thomas L., van Calsteren P., Quinif Y. and Caillon N.
1387 (2011) Speleothem record of the last 180 ka in Villars cave (SW France):
1388 Investigation of a large $\delta^{18}\text{O}$ shift between MIS6 and MIS5. *Quaternary Sci. Rev.*
1389 **30**, 130-146.
- 1390 Wang Z. G., Schauble E. A. and Eiler J. M. (2004) Equilibrium thermodynamics of
1391 multiply substituted isotopologues of molecular gases. *Geochim. Cosmochim.*
1392 *Acta* **68**, 4779-4797.
- 1393 Weyhenmeyer C. E., Burns S. J., Waber H. N., Aeschbach-Hertig W., Kipfer R., Loosli
1394 H. H. and Matter A. (2000) Cool glacial temperatures and changes in moisture
1395 source recorded in Oman groundwaters. *Science* **287**, 842-845.
- 1396 Wilson S. A., Dipple G. M., Power I. M., Thom J. M., Anderson R. G., Raudsepp M.,
1397 Gabities J. E. and Southam G. (2009) Carbon dioxide fixation within mine wastes
1398 of ultramafic-hosted ore deposits: Examples from the Clinton Creek and Cassiar
1399 Chrysotile deposits, Canada. *Econ. Geol.* **104**, 95-112.
- 1400 Wilson S. A., Barker S. L. L., Dipple G. M. and Atudorei V. (2010) Isotopic
1401 Disequilibrium during Uptake of Atmospheric CO₂ into Mine Process Waters:
1402 Implications for CO₂ Sequestration. *Environ. Sci. Technol.* **44**, 9522-9529.
- 1403 Zaarur S., Affek H. P. and Brandon M. (2013) A revised calibration of the clumped
1404 isotope thermometer. *Earth Planet. Sci. Lett.* **382**, 47-57
- 1405 Zeebe R. E. and Wolf-Gladrow D. A. (2001) *CO₂ in Seawater: Equilibrium, Kinetics,*
1406 *Isotopes.* Elsevier, Amsterdam.
1407

1408 **Figure Captions**

1409

1410 **Figure 1.** Location of hyperalkaline springs and associated travertine terraces where fresh
1411 carbonate precipitates and preserved travertines were sampled in this study (black dots).
1412 Samail ophiolite shown in green.

1413

1414 **Figure 2.** Photographs of hyperalkaline spring sampling sites and subsampled travertine
1415 terraces. (a) Hyperalkaline blue pools within streambed at Qafeefah. (b) Shallow flow of
1416 hyperalkaline fluids along the surface of travertine terraces at Al Bana, flow path
1417 sampling of carbonate and spring water at OM12_07V and OM12_07U. (c) Surface film
1418 (OM11_07V) and bottom floc (OM11_07U) from Misbit Spring pool. (d) Shallow flow
1419 of hyperalkaline fluids along the surface of travertine terraces at Al Hilayw, flow path
1420 sampling of spring water at OM12_09AA, OM12_09AB, OM12_09AC and sampling of
1421 fresh precipitates (bottom floc) at OM12_09AA. (e) Man-made elevated pool collecting
1422 alkaline spring water (OM10-6COPS) at Al Bana travertines. (f) Subsampled travertine
1423 terrace from Wadi Uqaybah (OM10-32C subsamples 8, 9, 10, 11).

1424

1425 **Figure 3.** Water data from hyperalkaline springs in Oman. (a) Distribution of water
1426 temperatures at multiple sites measured in January (this study; Paukert et al., 2012;
1427 Chavagnac et al., 2013b) and measured year-round at a single site (Neal and Stanger,
1428 1985). (b) Correlation between δD and $\delta^{18}O$ of spring water, shown relative to the global
1429 meteoric water line (GMWL) (Craig, 1961). (c) Distribution of $\delta^{18}O$ values of

1430 hyperalkaline spring water. (d) Distribution of $\delta^{13}\text{C}$ values of dissolved inorganic carbon
1431 in hyperalkaline springs.

1432

1433 **Figure 4.** Stable isotope variations in spring water and carbonate bottom flocc along flow
1434 paths at Al Bana, Al Hilayw, Falaj 1, and Falaj 2 travertines. There are no systematic
1435 variations in $\delta^{13}\text{C}$ in spring water DIC (panel A) or carbonate bottom flocc (panel C).
1436 Spring water $\delta^{18}\text{O}$ increases with distance along some flow paths (panel B) and is likely
1437 the result of evaporation along the flow path, which also results in enrichments in δD (as
1438 shown by the correlation between δD and $\delta^{18}\text{O}$ of spring water below the global meteoric
1439 water line (GMWL) (Craig, 1961) in panel E). Carbonate $\delta^{18}\text{O}$ in bottom flocc sampled
1440 along flow paths (panel D) does not show systematic variation with distance, $\delta^{18}\text{O}_{\text{water}}$, or
1441 water temperature (panel E).

1442

1443 **Figure 5.** Clumped isotope and stable isotope results for fresh precipitates (diamonds)
1444 and layered travertines (squares). Dashed boxes indicate the range of expected
1445 equilibrium values (Table 4). (a) $\delta^{18}\text{O}$ and $\delta^{13}\text{C}$ values of fresh precipitates and layered
1446 travertine in this study overlap with values from previous studies of Oman travertines
1447 (gray circles; Clark and Fontes, 1990; Clark et al., 1992; Kelemen et al., 2011; Mervine et
1448 al., 2014). $\delta^{18}\text{O}$ and $\delta^{13}\text{C}$ of fresh precipitates range from highly depleted values in
1449 surface films (pale blue diamonds) to more equilibrium-like values in bottom flocc (darker
1450 blue diamonds), and preserved travertines span a similar range of stable isotope
1451 compositions. (b) Clumped isotope compositions of fresh precipitates from alkaline
1452 springs range from enriched Δ_{47} values associated with depleted $\delta^{18}\text{O}$ values to

1453 compositions near expected equilibrium values. Layered travertines (gray squares) are
1454 shown for reference. (c) Clumped isotope compositions of layered travertines: recently-
1455 formed travertines from active hyperalkaline systems (green squares); subsamples of
1456 travertine terrace OM10-32C grouped by ^{14}C age (pink squares $<20\text{ky}$, medium red
1457 squares $\sim 30\text{ky}$, dark red squares $\sim 40\text{ky}$); subsamples of 40,000 year old travertine terrace
1458 OM10-78C (orange squares). Dotted lines in (b) and (c) indicate our first-order
1459 theoretical estimation of the $\Delta_{47}-\delta^{18}\text{O}$ slope associated with CO_2 hydroxylation
1460 (Appendix A).

1461

1462 **Figure 6.** Mixing trends in fresh precipitates from alkaline springs. Each panel shows
1463 $\Delta_{47}-\delta^{18}\text{O}$ mixing trends between the disequilibrium end-member (i.e., surface films) and
1464 several possible equilibrium end-members: (a) equilibrium with the lowest $\delta^{13}\text{C}$ values
1465 expected in soil CO_2 (carbonate $\delta^{13}\text{C}$ of -15‰ VPDB; Clark et al., 1992), (b) equilibrium
1466 with the atmospheric CO_2 (carbonate $\delta^{13}\text{C}$ of 0‰ VPDB; Clark et al., 1992), (c)
1467 equilibrium with the lowest $\delta^{18}\text{O}$ values observed in alkaline springs in Oman (water
1468 $\delta^{18}\text{O}$ -2.1‰ VSMOW; Neal and Stanger, 1985), (d) equilibrium with the highest $\delta^{18}\text{O}$
1469 values observed in alkaline springs in Oman (water $\delta^{18}\text{O}$ 2.5‰ VSMOW; this study).
1470 Dashed black boxes indicate the range of expected values at equilibrium (Table 4). The
1471 black dotted line shown in all panels represents mixing with an equilibrium end-member
1472 corresponding to the temperatures and isotopic compositions of alkaline spring water
1473 from Misbit Spring, and does not pass through the data points representing fresh
1474 carbonate precipitates from that specific spring (black crosses). Most bottom floc samples
1475 from larger pools record Δ_{47} values in excess of linear trends between the enriched

1476 disequilibrium values observed in surface films and values representing equilibrium with
1477 observed water temperatures. These trends are best explained by mixing between a
1478 disequilibrium end-member and an end-member formed in equilibrium with somewhat
1479 cooler temperatures (e.g., 17-25°C, corresponding to Δ_{47} values of 0.75-0.71‰) than
1480 those typically observed in hyperalkaline springs.

1481 **Figure 7.** Mixing trends in young subsamples of OM10-32C. Trends in $\delta^{18}\text{O}$, $\delta^{13}\text{C}$,
1482 fraction modern carbon, and Δ_{47} suggest subsamples of the layered travertine terrace
1483 OM10-32C with ages <20ky represent mixing of two isotopically distinct carbonate end-
1484 members. Sample symbols and dashed boxes denoting equilibrium conditions as in
1485 Figure 5. A mixing line (solid black line) between primary travertines with stable isotopic
1486 compositions similar to that of OM10-32C-9 and a hypothetical carbonate end-member
1487 with higher $\delta^{18}\text{O}$ and $\delta^{13}\text{C}$ and lower Δ_{47} (open black circle) reproduces the $\delta^{18}\text{O}$, $\delta^{13}\text{C}$,
1488 and Δ_{47} values observed in OM10-32C-8, OM10-32C-10, and OM10-32C when the
1489 assumed proportion of the hypothetical endmember in each of these subsample is 8%,
1490 43%, and 78%, respectively (panels A, C, D). Increases in fraction modern carbon would
1491 accompany increases in $\delta^{18}\text{O}$ and $\delta^{13}\text{C}$ due to mixing, but would not produce perfect
1492 correlations, as measured ^{14}C ages (panel B) are influenced both by mixing with the
1493 younger end-member and real differences in primary travertine ages.

1494

1495 **Figure 8.** Processes controlling the stable isotope compositions of carbonates formed at
1496 hyperalkaline springs (surface precipitates and bottom floc – gray diamonds, travertines –
1497 gray squares) can be distinguished by the Δ_{47} and $\delta^{18}\text{O}$ trends they produce (panel A), but
1498 largely overlap in $\delta^{18}\text{O}$ and $\delta^{13}\text{C}$ trends (panel B). These processes include: (1) CO_2

1499 hydroxylation produces enrichments in Δ_{47} and depletions $\delta^{18}\text{O}$ and $\delta^{13}\text{C}$ (yellow). (2)
1500 Partial equilibration of DIC in alkaline springs shifts isotopic composition of the resulting
1501 carbonates from the disequilibrium end-member towards equilibrium with ambient
1502 conditions (blue). (3) Mixing of isotopically distinct carbonate end-members results in
1503 mixing anomalies in clumped isotope composition. For example, alkaline pool bottom
1504 flocc can include mixtures of the high pH disequilibrium end-member and carbonate
1505 precipitated in equilibrium with surface runoff (green). Similarly, the mixing between the
1506 travertines and subsequent generations of carbonate that precipitate within the pore space
1507 of travertines (e.g., from pore waters with $\delta^{18}\text{O}$ enriched by evaporation) can also result
1508 in mixing anomalies in clumped isotope composition (red). (4) Carbonate
1509 recrystallization (dissolution and re-precipitation) and isotopic exchange in older
1510 travertines (orange).

1511

1512 **Figure B1.** Calculated “true” ages of travertine subsamples of nOM10-32C versus the
1513 assumed age of the hypothetical contaminant carbonate end-member (e.g. later
1514 generations of carbonate precipitated within travertine pore space). “Apparent”
1515 (measured) ^{14}C ages (dotted or dashed lines) are plotted for comparison with the
1516 calculated “true” ages (solid lines). The proportions of contaminant carbonate end-
1517 member used in the calculation of “true” ages are as calculated in Section 5.2.2 and
1518 shown in Figure 7: 8% in OM10-32C-8, 0% in OM10-32C-9, 43% in OM10-32C-10, and
1519 78% OM10-32C-11. Subsamples with significant proportions of the contaminant
1520 carbonate end-member may have “true” ages tens of thousands of years older than the
1521 apparent ^{14}C ages (e.g., OM10-32C-10 and OM10-32C-11). The apparent relative

1522 chronology of the travertine subsamples can also be substantially changed by mixing with
1523 later generations of carbonate. For example, the measured apparent ^{14}C ages suggest
1524 OM10-32C-9 is the oldest, followed by sample OM10-32C-8, OM10-32C-10, then
1525 OM10-32C-11, but depending on the age of the contaminating end-member, the “true”
1526 order of these OM10-32C subsamples could be 10, 9, 11, 8; 10, 9, 8, 11; or 9, 10, 8, 11.

Table 1. Surface carbonate samples associated with alkaline springs

Sample	Location	Type	UTM- E ^a	UTM- N ^a	¹⁴ C Age ^b	Ref. ^c	Major carb min ^d	Minor carb min ^e	Ref. ^f
<i>Fresh precipitates from alkaline springs - samples with clumped isotopes analyzed at WHOI</i>									
OM10-6COPS	Al Bana	Bottom floc, man-made	487316	2576132	>Modern	4	Calcite	Aragonite	4
OM12_07V	Al Bana	Bottom floc, shallow flow	489560	2575440			Calcite + aragonite		this study
OM12_07X2	Al Bana	Bottom floc, pool	489560	2575440			Calcite + aragonite		this study
OM12_09AA	Al Hilayw	Bottom floc, shallow flow	585880	2523240			Calcite, aragonite		this study
OM12_09AE	Al Hilayw	Bottom floc, shallow pool	585880	2523240			Calcite + aragonite		this study
OM11_07U	Misbit	Bottom floc, pool	625990	2576260			Calcite, aragonite		2
OM11_07V	Misbit	Surface film, pool	625990	2576260			Calcite, aragonite		2
OM11_07Y	Misbit	Bottom floc, wadi mixing	625990	2576260			Aragonite, calcite		2
OM09-6COPS	Qafeefah	Bottom floc, pool	646107	2533645	295	4	Aragonite	Calcite	4
OM09-7COPS	Qafeefah	Bottom floc, pool	646107	2533645	350	4	Aragonite	Calcite	4
OM10-1COPS	Qafeefah	Surface film	646117	2533648	>Modern	4	Calcite		4
OM10-2COPS	Qafeefah	Bottom floc, pool	646072	2533678	>Modern	4	Aragonite	Calcite	4
OM09-8COPS	Wadi Sudari	Bottom floc, pool	443118	2650078	>Modern	4	Calcite, aragonite		4
OM09-10COPS	Wadi Uqaybah	Surface film	426183	2633965	>Modern	4	Calcite		4
<i>Fresh precipitates from alkaline spring flow paths - samples with only $\delta^{13}\text{C}$ and $\delta^{18}\text{O}$ analyzed at University of Waterloo</i>									
OM12_07U	Al Bana	Bottom floc	489560	2575440					
OM12_07W1	Al Bana	Surface film	489560	2575440					
OM12_07W2	Al Bana	Bottom floc	489560	2575440					
OM12_07X1	Al Bana	Surface film	489560	2575440					
OM12_01A	Falaj	Bottom floc	608440	2525960					
OM12_01B	Falaj	Bottom floc	608440	2525960					
OM12_01C1	Falaj	Surface film	608440	2525960					
OM12_01C2	Falaj	Bottom floc	608440	2525960					
OM12_01D	Falaj	Bottom floc	608440	2525960					
OM12_01E1	Falaj	Bottom floc	608440	2525960					
OM12_01E2	Falaj	Surface film	608440	2525960					
OM12_01F1	Falaj	Surface film	608440	2525960					
OM12_01F2	Falaj	Bottom floc	608440	2525960					
OM12_01G1	Falaj	Surface film	608440	2525960					
OM12_01G2	Falaj	Bottom floc	608440	2525960					

Table 1. Surface carbonate samples associated with alkaline springs

Sample	Location	Type	UTM- E ^a	UTM- N ^a	¹⁴ C Age ^b	Ref. ^c	Major carb min ^d	Minor carb min ^e	Ref. ^f
<i>Travertine deposits</i>									
OM08-200	Kharma	Recent travertine	600173	2528469	305	1	Calcite		3
OM07-34c	Wadi Mahram	Recent travertine	608365	2526870	>Modern	1	Calcite		3
OM09-85C-MS	Wadi Sudari	Recent travertine	443082	2650304	>Modern	4	Calcite		4
OM09-89C-MS	Wadi Sudari	Recent travertine	443118	2650078	>Modern	4	Calcite	Aragonite	4
OM10-32C-1	Al Bana	Travertine terrace	487305	2576134	44700	4	Calcite		4
OM10-32C-2	Al Bana	Travertine terrace	487305	2576134	42500	4	Calcite		4
OM10-32C-6	Al Bana	Travertine terrace	487305	2576134	34040	4	Calcite	Dolomite	4
OM10-32C-8	Al Bana	Travertine terrace	487305	2576134	18350	this study	Calcite		4
OM10-32C-9	Al Bana	Travertine terrace	487305	2576134	32010	4	Calcite		4
OM10-32C-10	Al Bana	Travertine terrace	487305	2576134	15640	this study	Calcite		4
OM10-32C-11	Al Bana	Travertine terrace	487305	2576134	8890	4	Calcite		4
OM10-78C-3	Wadi Uqaybah	Travertine terrace	426266	2633919	41610	4	Calcite		4
OM10-78C-4	Wadi Uqaybah	Travertine terrace	426266	2633919	39530	4	Calcite	Dolomite	4
OM10-78C-6	Wadi Uqaybah	Travertine terrace	426266	2633919	37540	4	Calcite		4

^a UTM coordinates in Zone 40Q. Coordinates where both easting and northing end in zero are approximate, estimated to nearest 10 m.

^b Calibrated ¹⁴C age, years before present. By convention, "present" = 1950.

^c References for ¹⁴C ages: 1 - Kelement et al., 2011; 2 - Paukert et al., 2012; 3 - Falk, 2013; 4 - Mervine et al., 2014

^d Major carbonate minerals (> approx 20%), more abundant mineral listed first; Calcite + aragonite indicates roughly equal proportions

^e Minor carbonate minerals (< approx 10%)

^f References for mineralogy: 1 - Kelement et al., 2011; 2 - Paukert et al., 2012; 3 - Falk, 2013; 4 - Mervine et al., 2014

Table 2. Water data from alkaline springs

Sample ID ^a	Location	Site ^b	Dist., m ^c	pH	T °C	$\delta^{18}\text{O}$, ‰ VSMOW	$\delta^2\text{H}$, ‰ VSMOW	$\delta^{13}\text{C}_{\text{DIC}}$, ‰ VPDB	DIC, mmol/L ^d	Ca, mmol/L ^d	Mg, mmol/L ^d	Paukert ^e	Carbonate samples ^f
OM10_05AA	Al Bana	Aardvark		11.65	28.5	0.09	-0.85	-19.71	0.26	1.66	3.0E-02	√	
OM10_06AH	Al Bana	Al Ohwenah		11.16	38.4	-1.08	-4.08	-19.42	0.16	2.01	1.8E-02	√	
OM10_06AG	Al Bana	Al Thurawah		11.14	37.7	-0.42	-2.40	-17.82	0.18	1.54	9.4E-03	√	
OM09_W14H	Al Bana	Fork		12.08	26	0.54	-1.04	-11.66	0.20				
OM09_W14I	Al Bana	Gas Crack		11.84	32	1.89	-1.79	-13.24	0.22				
OM10_05AD	Al Bana	Gas Crack		11.68	32.6	1.15	-2.59	-14.8	0.22	2.11	3.3E-02	√	
OM10_05AF	Al Bana	Spine Mama		11.9	24.2	0.51	0.38	-23.67	0.26	1.57	2.7E-02	√	OM12_07X1,2
OM12_07X	Al Bana	Spine Mama	0	11.60	28.3	-0.62	-3.23	NA	0.12	1.60	BDL		OM12_07X1*,2**
OM12_07W	Al Bana	Papa	2.9	11.63	28.7	-0.61	-3.25	NA		1.83	BDL		OM12_07W1*,2*
OM12_07V	Al Bana	Sister	5.3	11.58	28.7	-0.63	-3.36	-18.36		1.78	BDL		OM12_07V**
OM12_07U	Al Bana	Brother	12.8	11.39	28.0	0.95	3.48	-26.82		0.57	BDL		OM12_07U*
OM08_W09	Al Hilayw			11.28		0.75	6.91						
OM08_W10	Al Hilayw			11.31		0.62	5.98						
OM08_W11	Al Hilayw			11.32		1.00	3.28						
OM08_W12	Al Hilayw			11.32		0.51	4.22						
OM08_W13	Al Hilayw			11.35		-0.21	1.08						
OM12_09AE	Al Hilayw	Land Cruiser	0	11.39	25.9	0.50	3.94	NA		1.49	BDL		OM12_09AE**
OM12_09AD	Al Hilayw	Camel	2.3	11.40	25.8	0.57	4.49	-24.11		1.51	BDL		
OM12_09AC	Al Hilayw	Sandal	6.8	11.41	24.8	0.64	4.82	-23.95		1.42	BDL		
OM12_09AB	Al Hilayw	Bedu Truck	12	11.43	24.1	1.00	6.38	NA		1.17	BDL		
OM12_09AA	Al Hilayw	Moped	17	11.31	22.5	1.63	9.24	-18.35		0.82	BDL		OM12_09AA**
OM09_W04F	Al Hilayw	Lungs		11.76	25.6	1.74	5.64	NA	0.22	1.40	8.6E-03	√	
OM09_W04G	Al Hilayw	Jimi		11.77	27.1	2.02	6.02	-28.73	0.02	1.31	9.1E-03	√	
OM09_W04H	Al Hilayw	Africa		11.51	24.5	2.50	9.75		0.78				
OM09_W04I	Al Hilayw	dnstr of Jimi		11.9	20.7	1.98	7.82	-21.38	0.20	1.07	9.7E-03	√	
OM08_W01	Bahla			11.49		0.59	4.91						
OM08_W 17	Dima			11.2		-0.18	0.30						
OM09_W06O	Dima	Pacman		11.54	30.3	0.52	-0.14	-12.99	0.16	1.82	7.2E-03	√	
OM08_W02	Falaj			10.5		-0.40	-0.55						
OM08_W03	Falaj			11.38		-0.35	0.53						
OM08_W04	Falaj			11.15		-0.29	-0.47						
OM08_W05	Falaj			11.38		-0.36	1.41						
OM09_W02A	Falaj 1	Falaj Spring		11.52	29.1	0.74	1.96	NA	0.18				
OM10_02L	Falaj 1	Falaj Spring		11.52	30.8	0.65	0.85	-17.42	0.20	1.83	2.5E-02	√	

Table 2. Water data from alkaline springs

Sample ID ^a	Location	Site ^b	Dist., m ^c	pH	T °C	$\delta^{18}\text{O}$, ‰ VSMOW	$\delta^2\text{H}$, ‰ VSMOW	$\delta^{13}\text{C}_{\text{DIC}}$, ‰ VPDB	DIC, mmol/L ^d	Ca, mmol/L ^d	Mg, mmol/L ^d	Paukert ^e	Carbonate samples ^f
OM12_01G	Falaj 1	Falaj Spring	0	11.25	30.3	-0.53	-1.16	-17.46	0.11	2.03	1.3E-02		OM12_01G1*,2*
OM12_01F	Falaj 1	Ogre	5.5	11.22		-0.48	-1.09	-16.07	0.09	2.07	BDL		OM12_01F1*,2*
OM12_01E	Falaj 1	Hobbit	11.5	11.35		-0.49	-1.14	-17.83	0.09	2.09	BDL		OM12_01E1*,2*
OM12_01D	Falaj 1	Elf	14.7	11.31		-0.51	-1.21	-18.71	0.10	2.11	BDL		OM12_01D*
OM12_01C	Falaj 1	Angry Worm	16.6	11.28		-0.48	-1.46	-18.00	0.11	2.10	BDL		OM12_01C1*,2*
OM12_01B	Falaj 1	Dwarf	19.5	11.25		-0.45	-0.93	-18.57	0.12	2.11	BDL		OM12_01B*
OM12_01A	Falaj 1	Little Knobby	24.5	11.24		-0.45	-1.02	-18.88	0.14	2.09	BDL		OM12_01A*
OM10_03R	Falaj 2	Little Mermaid		11.63	27.9	1.12	6.33	-16.78	0.16	1.67	3.7E-02	√	
OM12_02L	Falaj 2	Little Mermaid	0	11.21	29.2	-0.54	-1.08	NA	0.08	1.90	8.6E-03		
OM12_02K	Falaj 2	Flounder	3.5	11.27		-0.51	-0.93	-12.85	0.15	1.89	BDL		
OM12_02J	Falaj 2	Sebastian	5.9	11.28		-0.36	-0.25	-14.95	0.14	1.81	8.8E-03		
OM12_02I	Falaj 2	Ursula	10.2	11.27		-0.11	0.76	-22.86	0.18	1.52	1.0E-02		
OM12_02H	Falaj 2	Triton	13.7	11.32		-0.11	0.79	-21.30	0.15	1.45	BDL		
OM08_W 14	Masira			11.26		-1.65	-8.35						
OM09_W10U	Misbit	Misbit Spring		11.37	31.4	-1.11	-6.63	-15.11	0.38				OM11_07U,V
OM10_01A	Misbit	Misbit Spring		11.2	31.6	-1.39	-6.75	-5.96	0.24	2.12	1.7E-02	√	OM11_07U,V
		Misbit Spring		11.23	27.4								OM11_07U**,V**
		Misbit mixing		10.62	27.7								OM11_07Y**
OM08_W 18	Qafeefah			11.18		-0.52	0.79						
OM09_W05L	Qafeefah	Eden		11.89	23.8	0.39	-0.92	-20.76	0.38	1.66	6.5E-02	√	
OM10_04S	Qafeefah	Glazed Kidney		11.76	27.5	0.56	4.14	-13.71	0.18	1.75	1.9E-02	√	OM10-1COPS
OM10_04U	Qafeefah	Snail		11.71	24.9	0.28	2.38	-6.19	0.24	1.69	1.9E-02	√	
OM10_07AJ	Shumayt	The Triangle		11.46	33.4	-1.44	-3.49	-17.79	0.12	1.87	2.1E-02	√	
OM10_09AT	Sudari	Chain of Fools		11.61	30.4	-1.54	-6.36	-15.35	0.12	1.78	1.9E-02	√	
OM09_W15J	Uqaybah	Edwin I		11.25	17.6	-1.20	-6.60	-16.14				√	
OM09_W15K	Uqaybah	Edwin II		11.68	21.7	-0.86	-8.49	-13.71				√	

^a Rows without water sample ID numbers indicate field measurements.

^b Site names refer to individual pools at alkaline springs, including source pools and pools along flow paths

^c Distance from source spring along flow path over travertine surface.

^d Limits of detection: DIC - 0.02 mmol/L, Ca - 0.04 mmol/L, Mg - 4.10E-03 mmol/L

^e Check mark in "Paukert" column indicates that additional water chemistry data for this sample can be found in Paukert et al. (2012)

^f Carbonate samples listed in this column were collected at the same site as the corresponding water sample, but not necessarily at the same time. Single or double asterisk indicates that the carbonate was collected at the same time as the water sample:

* - carbonates with $\delta^{18}\text{O}$ and $\delta^{13}\text{C}$ analyses only (University of Waterloo), ** - carbonates with full clumped isotope analyses (WHOI).

Table 3. Stable and clumped isotope data in fresh precipitates and travertine deposits

Type	Sample	Major carb min	n	$\delta^{13}\text{C}$, ‰ VPDB	$\delta^{18}\text{O}$, ‰ VPDB	$\Delta 47$, ‰
<i>Fresh precipitates from alkaline springs - clumped isotope analyses (WHOI)</i>						
OM10-6COPS	Bottom floc, man-made	Calcite	7	-23.58 ± 0.15	-13.98 ± 0.11	0.826 ± 0.005
OM12_07V	Bottom floc, shallow flow	Calcite + aragonite	3	-24.47 ± 0.12	-16.40 ± 0.11	0.830 ± 0.009
OM12_07X2	Bottom floc, pool	Calcite + aragonite	6	-20.85 ± 0.23	-13.20 ± 0.09	0.883 ± 0.006
OM12_09AA	Bottom floc, shallow flow	Calcite, aragonite	3	-23.90 ± 0.16	-14.13 ± 0.13	0.816 ± 0.011
OM12_09AE	Bottom floc, shallow pool	Calcite + aragonite	6	-16.60 ± 0.11	-12.49 ± 0.09	0.819 ± 0.005
OM11_07U	Bottom floc, pool	Calcite, aragonite	6	-13.23 ± 0.05	-3.50 ± 0.04	0.771 ± 0.007
OM11_07V	Surface film	Calcite, aragonite	6	-27.17 ± 0.05	-16.70 ± 0.05	0.851 ± 0.006
OM11_07Y	Bottom floc, wadi mixing	Aragonite, calcite	3	-13.97 ± 0.02	-4.24 ± 0.09	0.757 ± 0.006
OM09-6COPS	Bottom floc, pool	Aragonite	3	-15.18 ± 0.18	-3.61 ± 0.33	0.750 ± 0.016
OM09-7COPS	Bottom floc, pool	Aragonite	4	-18.53 ± 0.07	-6.99 ± 0.09	0.820 ± 0.011
OM10-1COPS	Surface film	Calcite	6	-26.38 ± 0.03	-16.07 ± 0.30	0.851 ± 0.012
OM10-2COPS	Bottom floc, pool	Aragonite	6	-12.25 ± 0.12	0.22 ± 0.02	0.751 ± 0.007
OM09-8COPS	Bottom floc, pool	Calcite, aragonite	6	-21.42 ± 0.11	-10.33 ± 0.17	0.773 ± 0.008
OM09-10COPS	Surface film	Calcite	3	-23.44 ± 0.35	-14.44 ± 0.03	0.844 ± 0.014
<i>Fresh precipitates from alkaline spring flow paths - $\delta^{13}\text{C}$ and $\delta^{18}\text{O}$ analyses only (University of Waterloo)</i>						
OM12_07U	Bottom floc		2	-24.54	-16.63	
OM12_07V	Bottom floc		1	-22.99	-16.90	
OM12_07W1	Surface film		2	-24.73	-16.12	
OM12_07W2	Bottom floc		2	-22.60	-15.68	
OM12_07X1	Surface film		2	-25.76	-16.36	
OM12_07X2	Bottom floc		2	-25.13	-12.25	
OM12_01A	Bottom floc		1	-14.90	-6.23	
OM12_01B	Bottom floc		2	-14.59	-4.65	
OM12_01C1	Surface film		1	-21.34	-16.88	
OM12_01C2	Bottom floc		2	-14.35	-5.97	
OM12_01D	Bottom floc		2	-14.06	-4.67	
OM12_01E1	Bottom floc		2	-14.49	0.08	
OM12_01E2	Surface film		1	-24.41	-18.41	
OM12_01F1	Surface film		2	-24.31	-12.99	
OM12_01F2	Bottom floc		2	-10.52	3.14	
OM12_01G1	Surface film		2	-23.58	-14.65	
OM12_01G2	Bottom floc		1	-19.93	-11.76	
<i>Travertine deposits - clumped isotope analyses (WHOI)</i>						
OM08-200	Modern travertine	Calcite	3	-19.98 ± 0.26	-12.06 ± 0.14	0.828 ± 0.007
OM07-34c	Modern travertine	Calcite	6	-25.35 ± 0.06	-15.42 ± 0.04	0.855 ± 0.008
OM09-85C	Modern travertine	Calcite	2	-24.89 ± 0.07	-14.25 ± 0.01	0.839 ± 0.003
OM09-89C	Modern travertine	Calcite	2	-21.85 ± 0.15	-12.05 ± 0.14	0.784 ± 0.019
OM10-32C-1	Travertine terrace	Calcite	3	-17.84 ± 0.05	-7.57 ± 0.05	0.705 ± 0.014
OM10-32C-2	Travertine terrace	Calcite	3	-14.87 ± 0.07	-6.50 ± 0.04	0.675 ± 0.006
OM10-32C-6	Travertine terrace	Calcite	3	-20.75 ± 0.04	-10.60 ± 0.02	0.675 ± 0.006
OM10-32C-8	Travertine terrace	Calcite	3	-16.64 ± 0.15	-9.16 ± 0.13	0.805 ± 0.011
OM10-32C-9	Travertine terrace	Calcite	3	-18.13 ± 0.06	-10.32 ± 0.03	0.787 ± 0.014
OM10-32C-10	Travertine terrace	Calcite	3	-10.87 ± 0.06	-3.86 ± 0.03	0.830 ± 0.010
OM10-32C-11	Travertine terrace	Calcite	3	-3.76 ± 0.07	0.58 ± 0.05	0.790 ± 0.007
OM11-78C-3	Travertine terrace	Calcite	3	-18.80 ± 0.04	-11.67 ± 0.01	0.795 ± 0.003
OM11-78C-4	Travertine terrace	Calcite	3	-19.68 ± 0.43	-12.57 ± 0.30	0.794 ± 0.010
OM11-78C-6	Travertine terrace	Calcite	3	-5.28 ± 0.07	-3.70 ± 0.06	0.695 ± 0.003

All values corrected to carbonate standards for clumped isotope analyses, as described in text.

Reported uncertainties for clumped isotope data are 1-S.E. of replicate measurements.

External precision for bulk stable isotope compositions measured at the University of Waterloo is 0.2‰ (1-S.D.) for $\delta^{18}\text{O}$ and 0.1‰ (1-S.D.) for $\delta^{13}\text{C}$.

Table 4. Possible carbonate mixing end-members for bottom flocc

	T, °C ^a	Δ_{47} , ‰ ^b	Water $\delta^{18}\text{O}$, ‰ ^c VSMOW ^c	Carbonate $\delta^{18}\text{O}$, ‰ ^d VPDB ^d	Carbonate $\delta^{13}\text{C}$, ‰ ^e VPDB ^e	End-member Abbrev.
Disequilibrium end-member	N/A	0.851	N/A	-16.7	-27	DIS
<i>Equilibrium end-members:</i>						
Carbon from soil CO ₂	17	0.750	-2.1	-2.8	-15	EM1-1
	17	0.750	2.5	1.8	-15	EM1-2
	39	0.643	-2.1	-7.4	-15	EM1-3
	39	0.643	2.5	-2.8	-15	EM1-4
Carbon from atmospheric CO ₂	17	0.750	-2.1	-2.8	0	EM2-1
	17	0.750	2.5	1.8	0	EM2-2
	39	0.643	-2.1	-7.4	0	EM2-3
	39	0.643	2.5	-2.8	0	EM2-4
Misbit Spring	32	0.681	-1.4	-5.0	-6	MS

^a Minimum and maximum temperatures observed in alkaline springs in Oman (17 and 39°C, respectively; Table 2; Paukert et al., 2012; Chavagnac et al., 2013b) are used to define extreme equilibrium end-members. Measured temperature in Misbit Spring in 2010 (water sample OM10_01A).

^b Expected Δ_{47} values (Ghosh et al., 2006) for given equilibrium end-member temperature; measured Δ_{47} value in OM11_07V used as representative disequilibrium end-member

^c Minimum and maximum $\delta^{18}\text{O}$ values observed in alkaline spring water in Oman (-2.1 and 2.5‰ VSMOW, respectively; Table 2; Neal and Stanger, 1985) used to define extreme equilibrium end-members. Measured spring water $\delta^{18}\text{O}$ in Misbit Spring (OM10_01A).

^d Expected carbonate $\delta^{18}\text{O}$ in equilibrium with given $\delta^{18}\text{O}_{\text{water}}$ value and temperature (Kim and O'Neil, 1997). Measured value in OM11_07V used for disequilibrium end-member.

^e Extreme end-members defined by minimum and maximum expected carbonate $\delta^{13}\text{C}$ in equilibrium with carbon from soil CO₂ and atmospheric CO₂, respectively. Expected carbonate $\delta^{13}\text{C}$ in equilibrium with soil CO₂ ranges from approximately -15 to -6‰ VPDB, while expected carbonate $\delta^{13}\text{C}$ in equilibrium with atmospheric CO₂ ranges from approximately -3 to 0‰ VPDB (Clark et al., 1992). Measured $\delta^{13}\text{C}_{\text{DIC}}$ in Misbit Spring (water sample OM10_01A). Measured value in OM11_07V used for disequilibrium end-member.

Table B.1. Calculated "true" ages of travertine subsamples

Sample			Measured ¹⁴ C		Max. contaminant Fm		Min. contaminant Fm	
Sample Name	Type	% Secondary end-member	Fm	¹⁴ C age	"True" Fm	¹⁴ C age	"True" Fm	¹⁴ C age
Hypothetical	Contaminating end-member	100			0.462	7100	0.369	8890
OM10-32C-11	Mixed travertine	78.0	0.369	8890	0.040	30140	0.369	8890
OM10-32C-10	Mixed travertine	42.8	0.198	15640	0.000	>50000	0.069	25760
OM10-32C-8	Mixed travertine	8.2	0.153	18350	0.125	20160	0.133	19550
OM10-32C-9	Travertine end-member	0	0.031	32010				

Figures

Figure. 1



Figure 2.

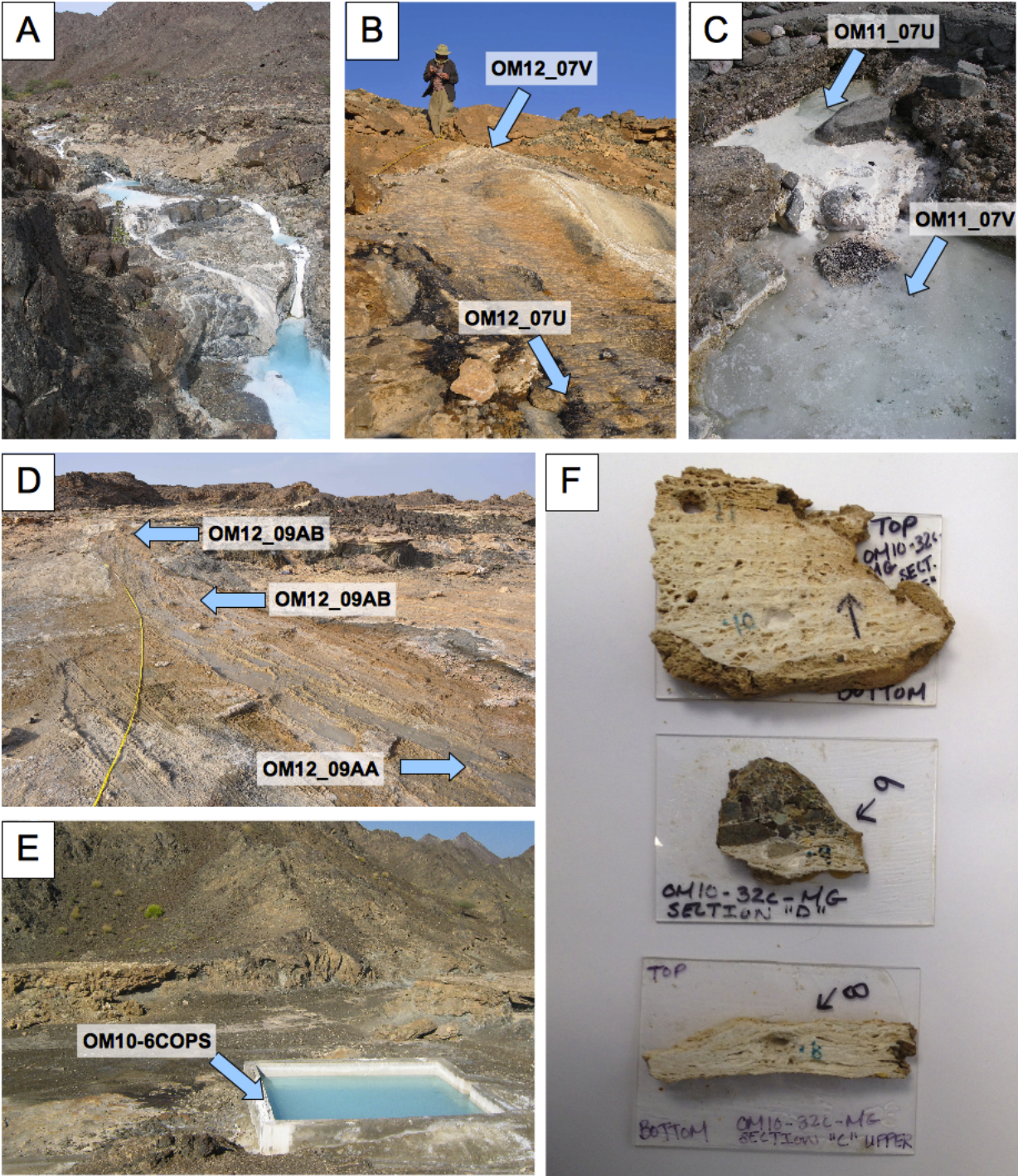


Figure 3.

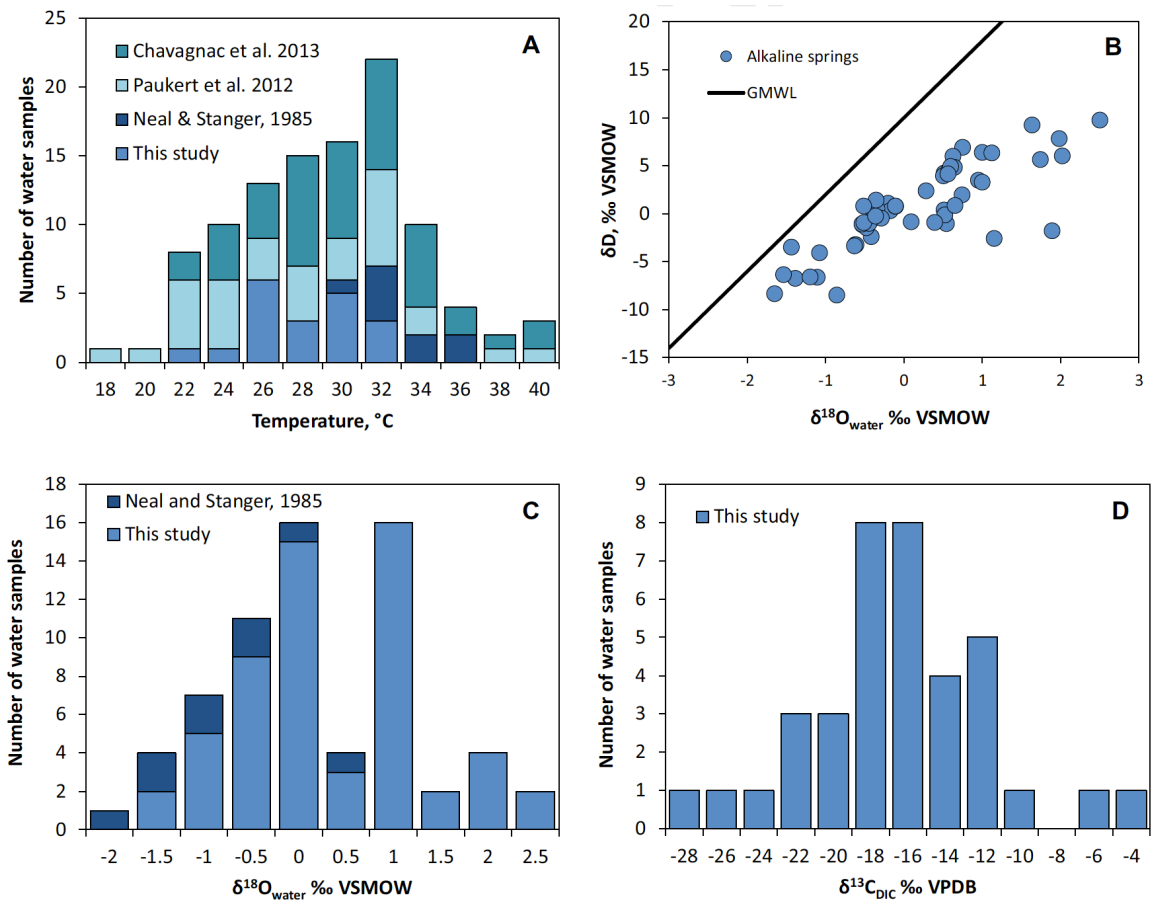


Figure 4.

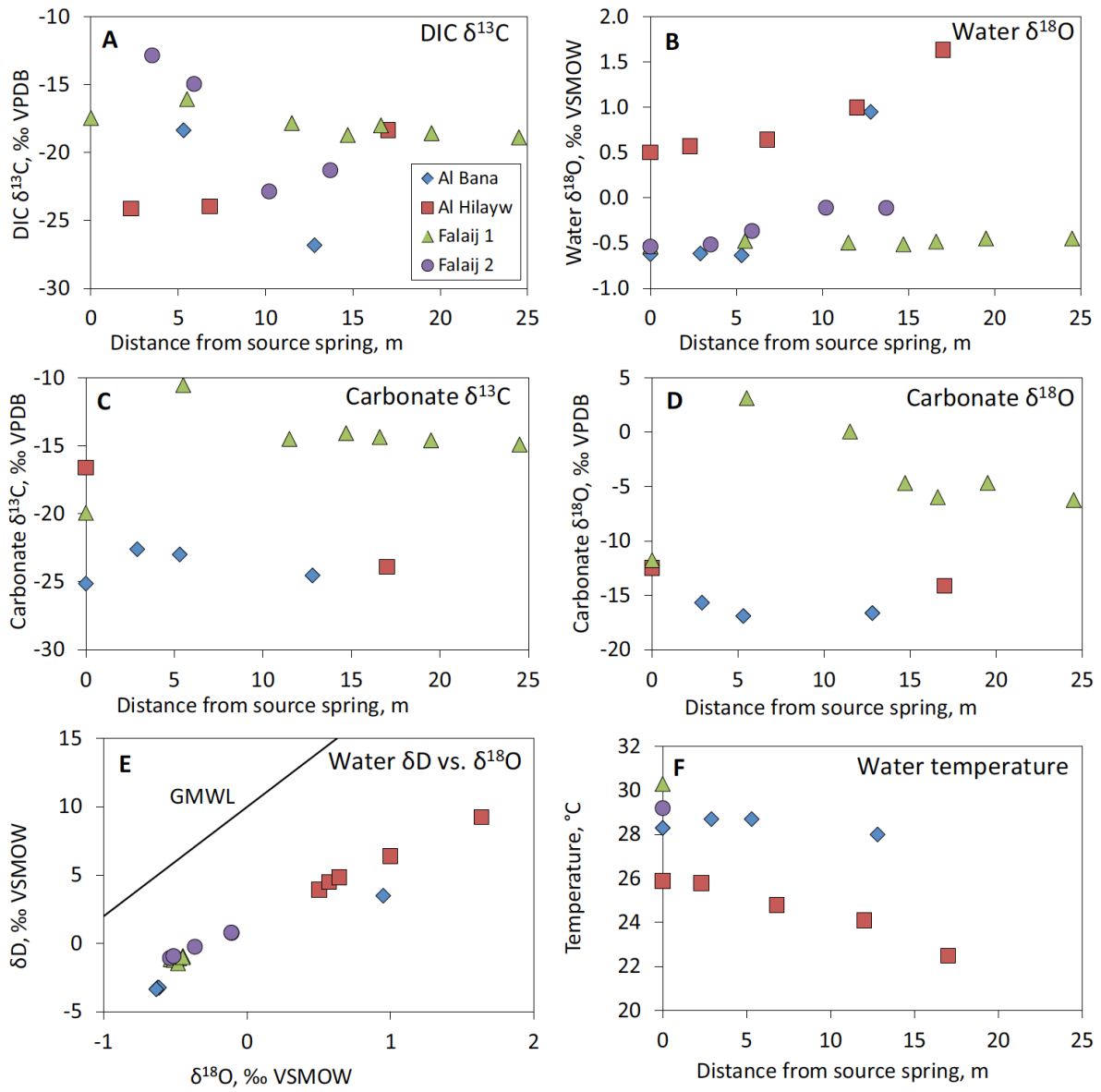


Figure 5.

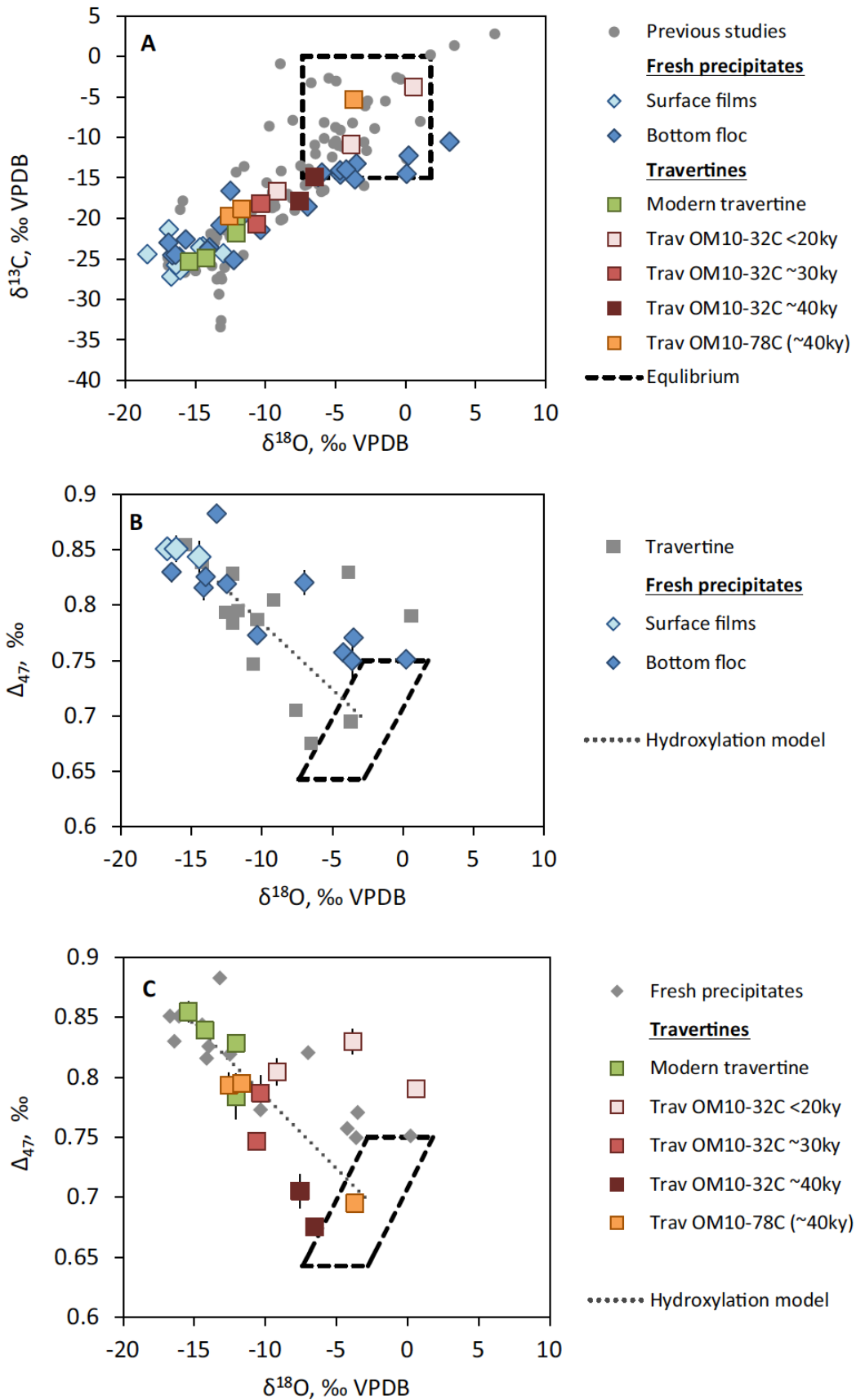


Figure 6.

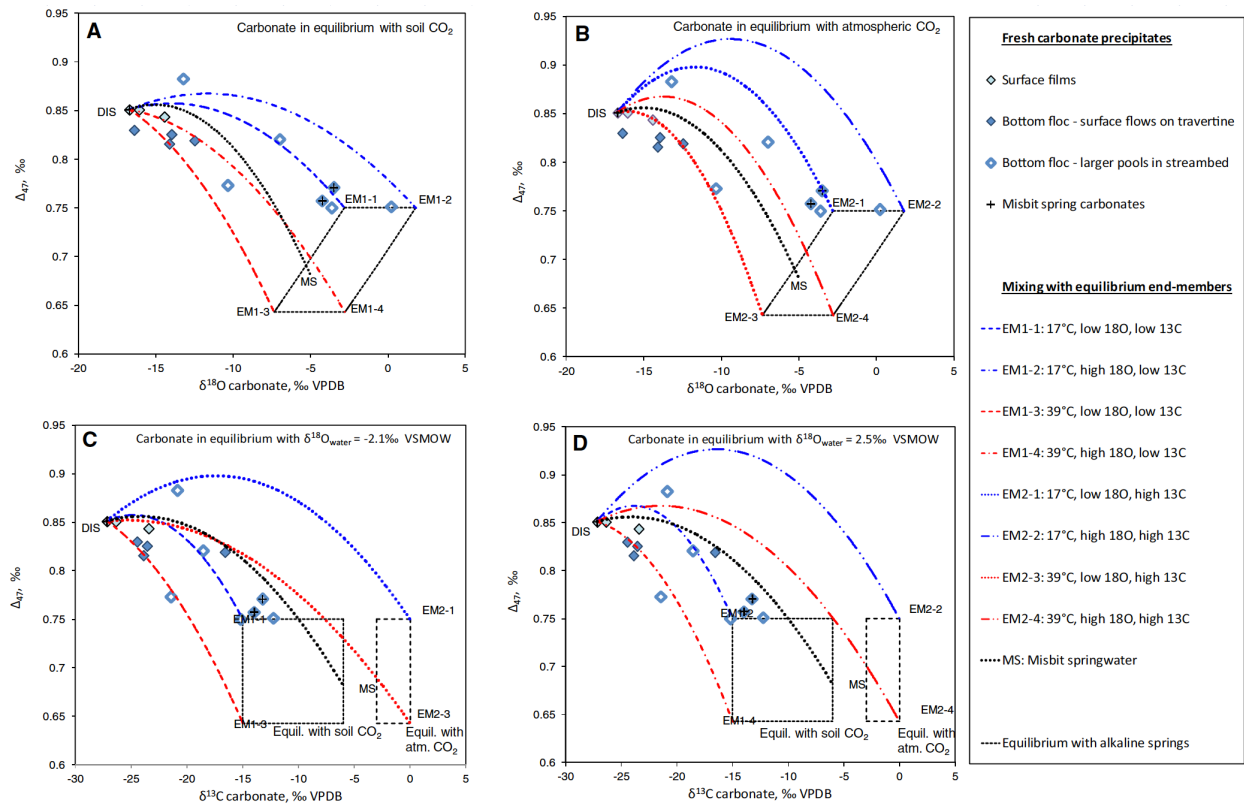


Figure 7.

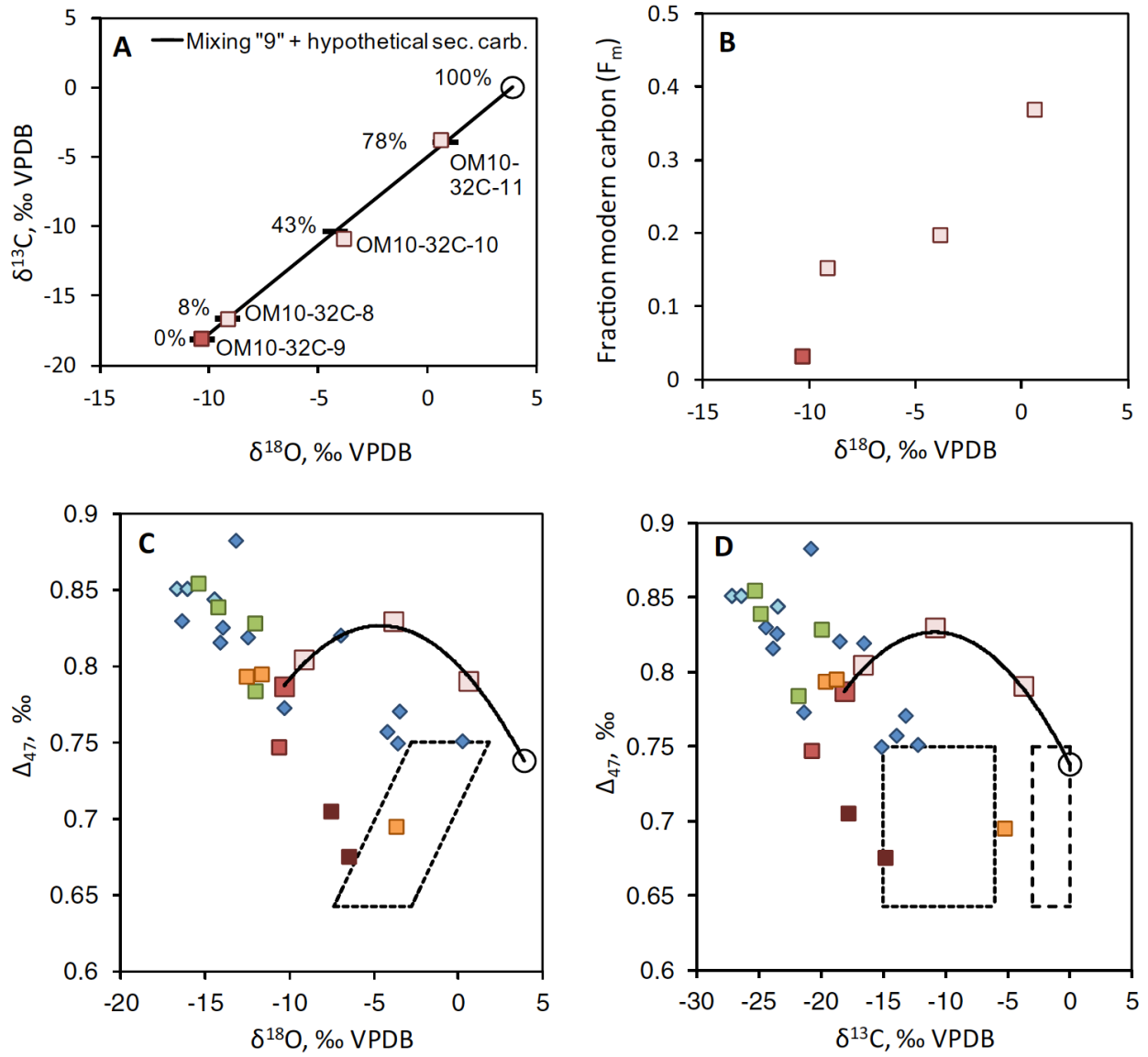


Figure 8.

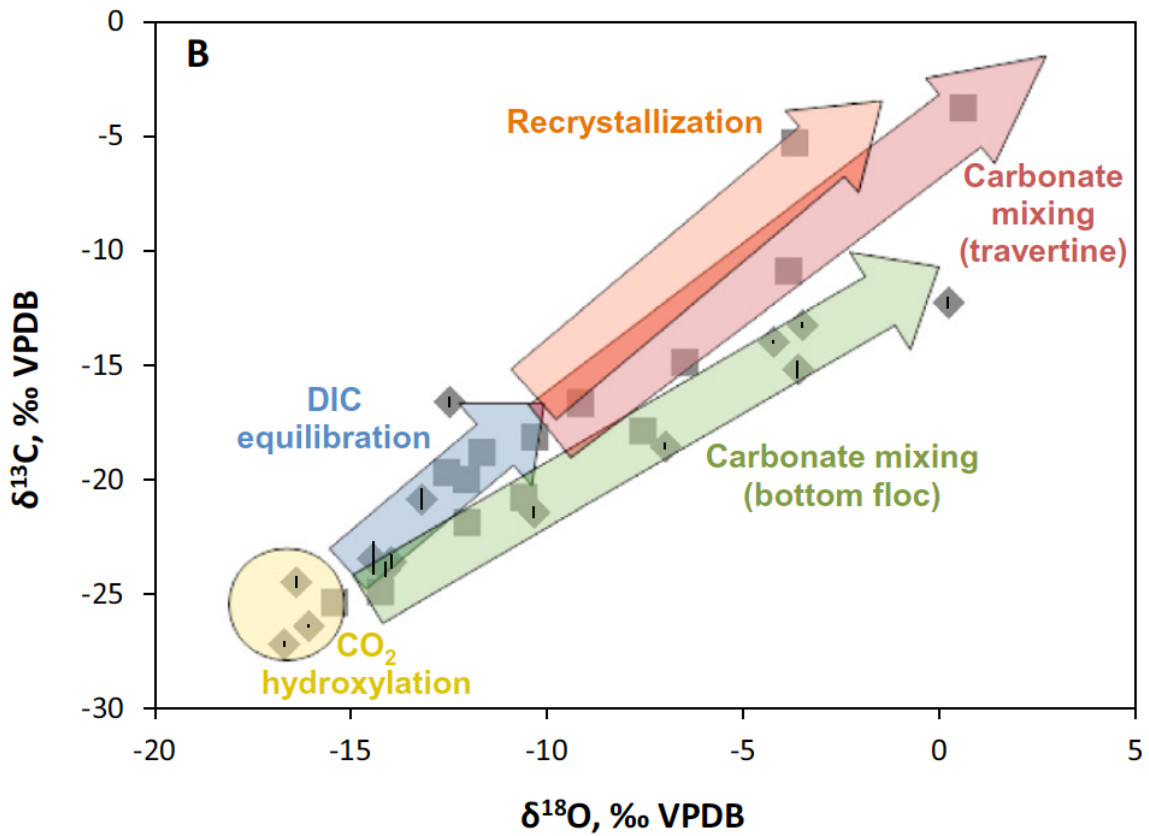
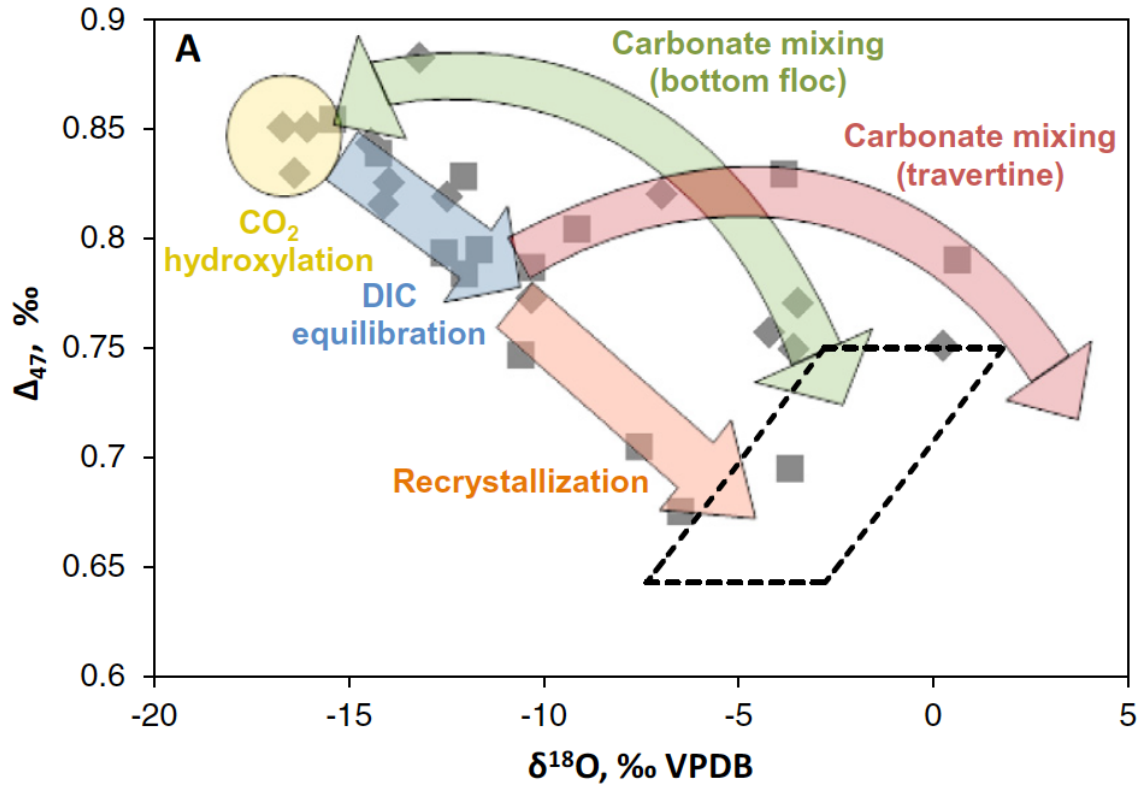
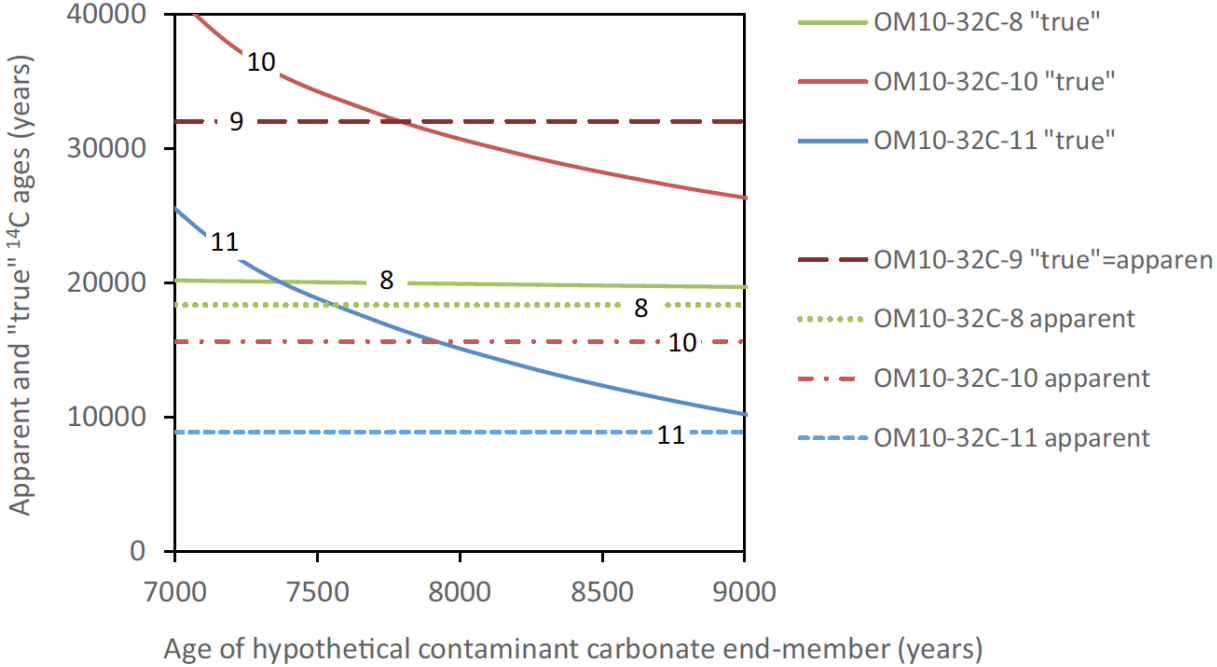
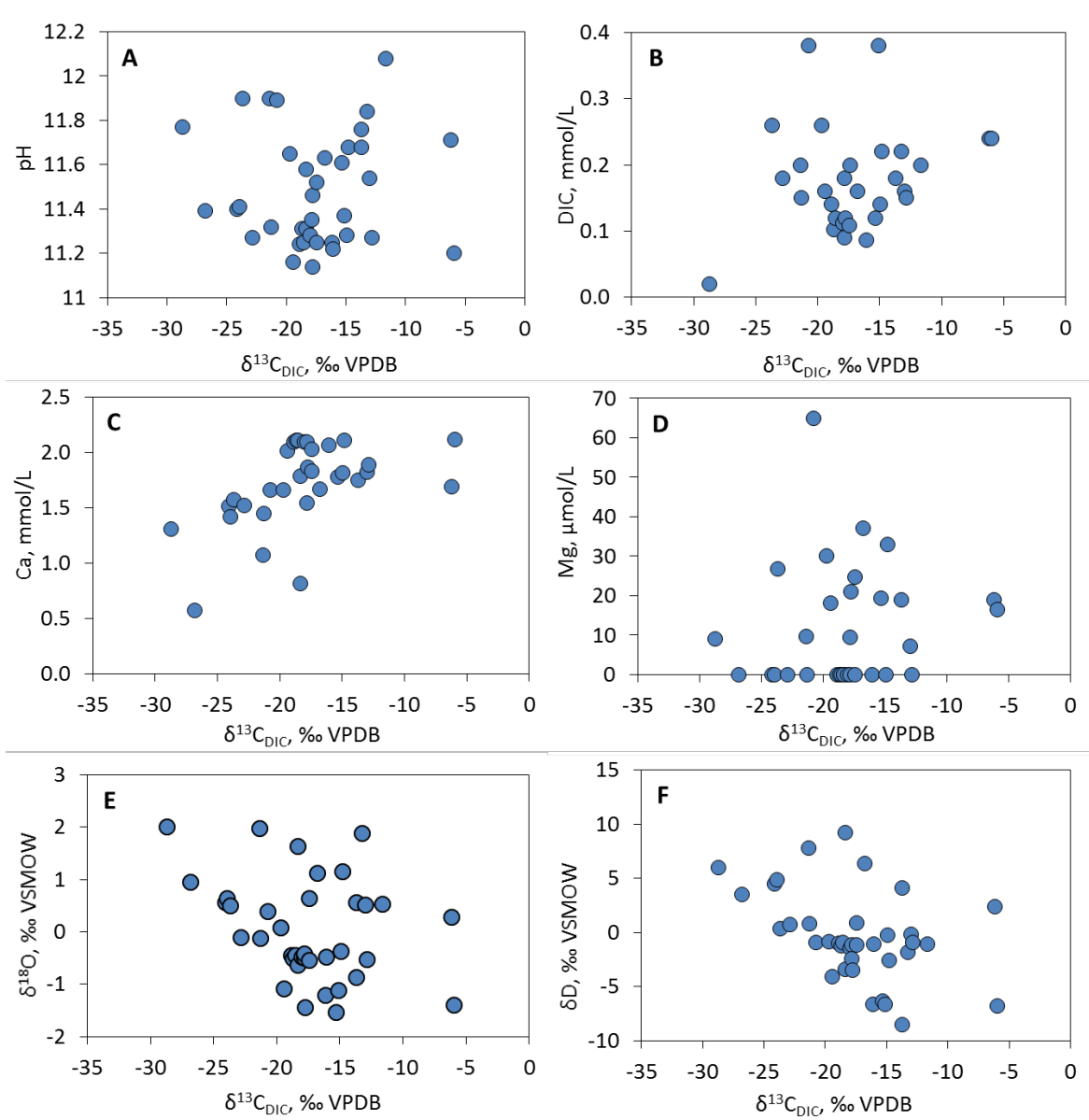
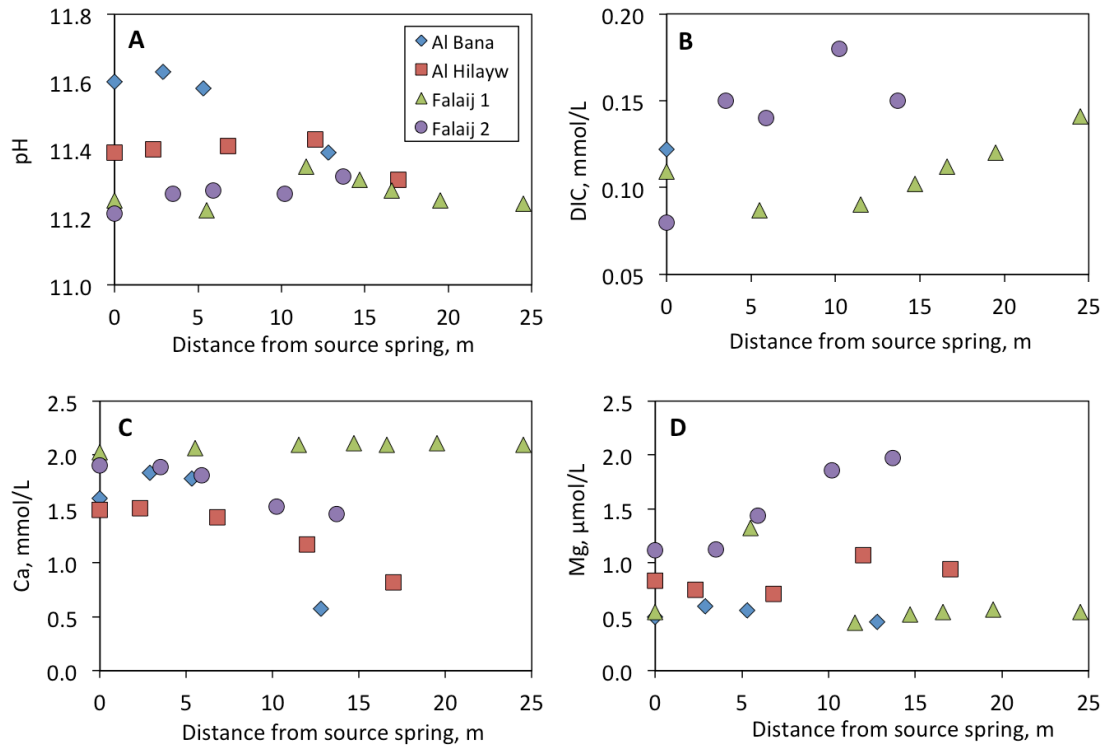


Figure B.1.

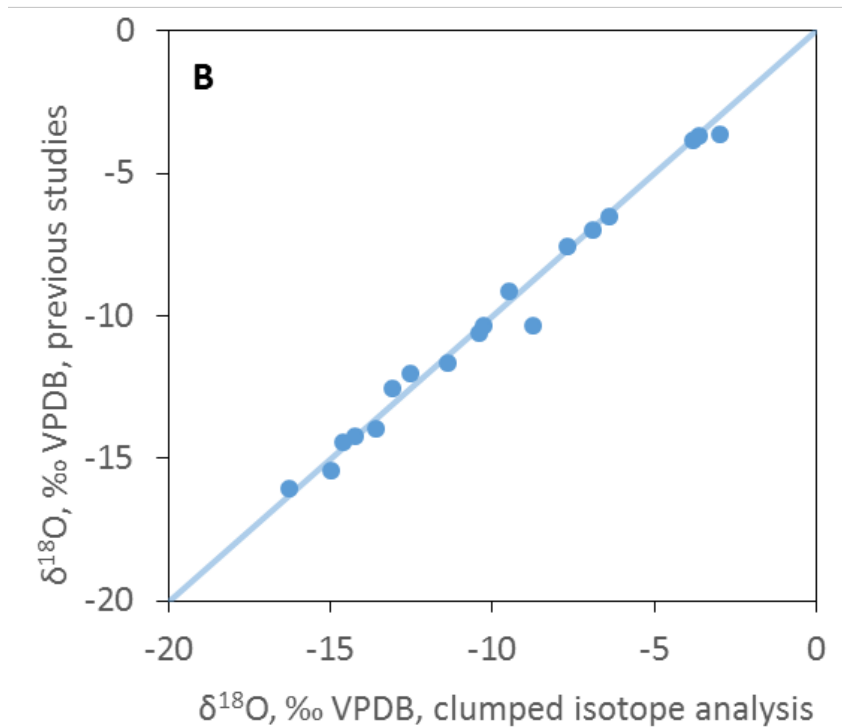
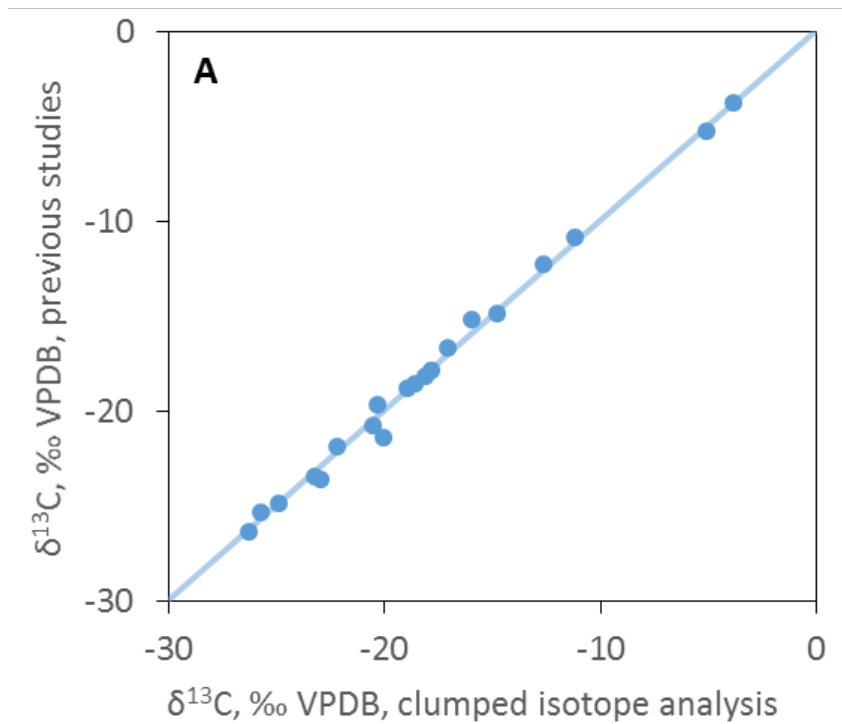




Supplementary Figure S1. Variations in hyperalkaline spring water chemistry and stable isotope compositions plotted against $\delta^{13}\text{C}_{\text{DIC}}$.



Supplementary Figure S2. Variations in hyperalkaline spring water chemistry with distance from the source spring in shallow flows along the surface of travertine terraces.



Supplementary Figure S3. The $\delta^{13}\text{C}$ (A) and $\delta^{18}\text{O}$ (B) values of fresh carbonate precipitates and preserved travertines obtained by clumped isotope analysis at WHOI are both in excellent agreement with previously reported bulk stable isotope compositions of these samples (Kelemen et al., 2011; Mervine et al., 2014).